858 *Inorg. Chem.* **2011**, *50*, 858–872
DOI: 10.1021/ic101455z

Inorganic Chemistry
Article

Sulfates of the Refractory Metals: Crystal Structure and Thermal Behavior of $Nb_2O_2(SO_4)_3$, $MoO_2(SO_4)$, $WO(SO_4)_2$, and Two Modifications of $Re_2O_5(SO_4)_2$

Ulf Betke and Mathias S. Wickleder*

Institute for Pure and Applied Chemistry, Carl von Ossietzky University of Oldenburg, Carl-von-Ossietzky-Strasse 9-11, 26129 Oldenburg, Germany

Received July 21, 2010

The sulfates $Nb_2O_2(SO_4)_3$, $MoO_2(SO_4)$, $WO(SO_4)_2$, and two modifications of $Re_2O_5(SO_4)_2$ have been synthesized by the solvothermal reaction of $NbCl_5$, $WOCl_4$, $Re_2O_7(H_2O)_2$, and MoO_3 with sulfuric acid/SO_3 mixtures at temperatures between 200 and 300 °C. Besides the X-ray crystal structure determination of all compounds, the thermal behavior was investigated using thermogravimetric studies. $WO(SO_4)_2$ (monoclinic, $P2_1/n$, $a = 7.453(1)$ Å, $b = 11.8232(8)$ Å, $c = 7.881(1)$ Å, $\beta = 107.92(2)°$, $V = 660.7(1)$ Å^3, $Z = 4$) and both modifications of $Re_2O_5(SO_4)_2$ (I: orthorhombic, *Pba*2, $a = 9.649(1)$ Å, $b = 8.4260(8)$ Å, $c = 5.9075(7)$ Å, $V = 480.27(9)$ Å^3, $Z = 2$; II: orthorhombic, *Pbcm*, $a = 7.1544(3)$ Å, $b = 7.1619(3)$ Å, $c = 16.8551(7)$ Å, $V = 863.64(6)$ Å^3, $Z = 4$) are the first structurally characterized examples of tungsten and rhenium oxide sulfates. Their crystal structure contains layers of sulfate connected [W═O] moieties or [Re_2O_5] units, respectively. The cohesion between layers is realized through weak M−O contacts (343−380 pm). $Nb_2O_2(SO_4)_3$ (orthorhombic, $Pna2_1$, $a = 9.9589(7)$ Å, $b = 11.7983(7)$ Å, $c = 8.6065(5)$ Å, $V = 1011.3(1)$ Å^3, $Z = 4$) represents a new sulfate-richer niobium oxide sulfate. The crystal structure contains a three-dimensional network of sulfate connected [Nb═O] moieties. In $MoO_2(SO_4)$ (monoclinic, *I*2/*a*, $a = 8.5922(6)$ Å, $b = 12.2951(6)$ Å, $c = 25.671(2)$ Å, $\beta = 94.567(9)°$, $V = 2703.4(3)$ Å^3, $Z = 24$) [MoO_2] units are connected through sulfate ions to a three-dimensional network, which is pervaded by channels along [100] accommodating the terminal oxide ligands. In all compounds except $WO(SO_4)_2$, the metal ions are octahedrally coordinated by monodentate sulfate ions and oxide ligands forming short M═O bonds. In $WO(SO_4)_2$, the oxide ligand and two monodentate and two bidentate sulfate ions build a pentagonal bipyramid around W. The thermal stability of the sulfates decreases in the order Nb > Mo > W > Re; the residues formed during the decomposition are the corresponding oxides.

1. Introduction

The name "refractory metals" is commonly used for metals which are characterized by high melting and boiling points as well as distinctive chemical inertness due to the formation of an oxidic passive layer. In engineering, refractory metals are mainly the elements niobium, tantalum, molybdenum, tungsten, and rhenium. All of these metals form their most stable compounds in the highest possible oxidation state of +V to +VII. Nonetheless, a broad range of chemistry of substances containing low valent refractory metals is known. In contrast to the large bulk of comprehensively characterized compounds of the refractory elements like chalcogenides, halogenides, and coordination and organometallic compounds in varying oxidation states, the number of structurally characterized (particular binary) compounds containing complex oxo-anions is astonishingly low.[1]

Reactions of refractory metals with sulfuric acid were reported several times, but detailed characterizations of sulfates of high valent refractory elements are rather scarce. The only binary sulfates for which crystal structure has been determined are $MoO_2(SO_4)$, already reported by Shultz-Sellack in 1871 but not structurally characterized until 2001 by Christiansen et al.,[2,3] and $Nb_2O_3(SO_4)_2 \cdot 0.25H_2O$, described by Boström et al. in 2004.[4,5] While $Nb_2O_3(SO_4)_2 \cdot 0.25H_2O$ probably needs revision as a result of our own investigations, the former seems to adopt three different modifications. However, Christiansen et al. determined only the structure of the orthorhombic modification with high accuracy. The crystal structure of a monoclinic one could be solved but it suffers from the poor quality of the single crystals. The third modification was assumed with respect to powder diffraction data. The formation of other compounds with oxo-anions of high valent refractory metals was

*To whom correspondence should be addressed. E-mail: mathias.wickleder@uni-oldenburg.de.

(1) Pollack, S. S. *Inorg. Chem.* **1987**, *26*, 1825–1826.
(2) Shultz-Sellack, C. *Chem. Ber.* **1871**, *4*, 12–15.
(3) Christiansen, A. F.; Fjellvåg, H.; Kjekshus, A.; Klewe, B. *J. Chem. Soc., Dalton Trans.* **2001**, *6*, 806–815.
(4) Ewald, B.; Prots, Y.; Boström, M. *Z. Kristallogr., New Cryst. Struct.* **2004**, *219*, 89–90.
(5) Boström, M.; Gemmi, M.; Schnelle, W.; Eriksson, L. *J. Solid State Chem.* **2004**, *177*, 1738–1745.

 Published on Web 01/05/2011

claimed but has never been proven. For example, Hayek et al. were able to synthesize the oxide sulfates $Nb_2O(SO_4)_4$, $MoO(SO_4)_2$, and $WO(SO_4)_2$ and the sulfate $Ta_2(SO_4)_5$ as white, extremely hygroscopic powders by reaction of the corresponding metal chlorides with SO_3 in sulfuryl chloride.[6,7] $Ta_2(SO_4)_5$ was also obtained by Goroshchenko and Andreeva in the system $Ta_2O_5/H_2SO_4/SO_3$.[8] The element distribution in these compounds was determined using elemental analysis or thermogravimetric measurements. There are no reliable structural data available.

Due to their high dielectricity constants, Nb_2O_5 and Ta_2O_5 are especially auspicious candidates for capacitor dielectric materials in complementary metal−oxide semiconductors (CMOS). New gate oxide materials are an essential step in the realization of Moore's Law of miniaturization in future semiconductors. For this reason, thermally labile compounds of the refractory elements have recently attracted intense interest as precursors for the deposition of thin metal−oxide layers. Actually, layers of Nb_2O_5 and Ta_2O_5 are prepared using techniques like metal−organic chemical vapor deposition (MOCVD), atomic layer deposition (ALD), and pulsed laser deposition (PLD).[9] Typical compounds used in these processes are volatile materials like chlorides, alkoxides, and more recently amides.[10,11] The big disadvantage of these methods is contamination of the deposited oxide layer with remarkable amounts of impurities, especially carbon.

In the search for carbon-free precursors for refractory metal oxides, we have started to extend our knowledge of the chemistry of precious metals and rare earth elements with complex oxo-anions.[12−15] Hence, we began investigating compounds of the refractory elements containing complex oxo-anions such as nitrates, perchlorates, and sulfates. Here, we report the crystal structure and the thermal decomposition of new oxide sulfates of refractory elements with the examples of $Nb_2O_2(SO_4)_3$, $WO(SO_4)_2$, and two modifications of $Re_2O_5(SO_4)_2$. Furthermore, we provide a new synthetic approach to $MoO_2(SO_4)$ leading to well-developed single crystals suitable for X-ray crystallography.

2. Experimental Section

2.1. Synthesis. All reactions were carried out in sealed glass ampules of 25 cm in length and 2 cm in diameter, which were heated in a block thermostat (Gefran 800P, Liebisch, Bielefeld, Germany), allowing the programming of designated heating and cooling rates. The glass ampules were charged with the starting materials in a glovebox under an inert atmosphere and then sealed under vacuum conditions with a CH_4/O_2 flame.

$Nb_2O_2(SO_4)_3$. A solution of 0.5 g of $NbCl_5$ (99%, Alfa-Aesar, Karlsruhe, Germany) in 2 mL of fuming sulfuric acid containing 25% SO_3 (puriss. Merck, Darmstadt, Germany) was heated to 200 °C for 48 h and then cooled to room temperature at a cooling rate of 2.5 °C/h. In this way, colorless single crystals of $Nb_2O_2(SO_4)_3$ suitable for X-ray diffraction could be grown. The glass ampule was opened in a glovebox under a nitrogen atmosphere, and the mother liquor was separated from the crystals by decantation. The crystals for X-ray diffraction were selected under inert oil (perfluorinated polyether, ABCR, Karlsruhe, Germany). For the DTA/TG measurements, the precipitate was washed with absolute tetrahydrofuran and dried *in vacuo* to remove the last traces of adhesive sulfuric acid.

$MoO_2(SO_4)$. A mixture of 1 g of MoO_3 (99.9%, Alfa-Aesar, Karlsruhe, Germany) and 1.5 mL of concentrated sulfuric acid (pure, BüFa, Oldenburg, Germany) was heated to 300 °C for 72 h followed by slow cooling to room temperature (2.5 °C/h). For satisfying crystal growth, it is essential that the water generated during the reaction is able to pass out of the system, which is easily achieved by leaving the ampule open to the atmosphere. In this way, colorless needles of several millimeters in length can be grown. Crystals for X-ray diffraction and the material used in DTA/TG measurements were prepared as described above for $Nb_2O_2(SO_4)_3$.

$WO(SO_4)_2$. A solution of 0.5 g of $WOCl_4$ in 1 mL of fuming sulfuric acid containing 65% SO_3 (puriss. Merck, Darmstadt, Germany) was heated to 200 °C for 48 h. Slow cooling of the resulting mixture to room temperature (2.5 °C/h) leads to small colorless single crystals. Crystals for X-ray diffraction and the material used in DTA/TG measurements were prepared as described above for $Nb_2O_2(SO_4)_3$. The reactant $WOCl_4$ was prepared according to literature methods by heating a suspension of WO_3 (99.8%, Alfa-Aesar, Karlsruhe, Germany) in thionyl chloride to 200 °C in a sealed glass ampule for 8 h.[16] After evaporation to dryness, the $WOCl_4$ was purified through sublimation under reduced pressure.

$Re_2O_5(SO_4)_2$−I. A suspension of metallic Re (H. C. Starck, Goslar, Germany) in fuming sulfuric acid (65% SO_3) was heated to 200 °C. On cooling, a small amount of pale yellow crystals separated from the mother liquor. A more convenient synthesis is the reaction of 0.75 g of $Re_2O_7(H_2O)_2$ ("solid perrhenic acid") with 2 mL of fuming sulfuric acid (65% SO_3) at 200 °C followed by slow cooling to room temperature (2.5 °C/h).

$Re_2O_5(SO_4)_2$−II. A solution of 0.5 g of $Re_2O_7(H_2O)_2$ in 1 mL of fuming sulfuric acid (65% SO_3) was heated to 300 °C followed by slow cooling to room temperature (2.5 °C/h). In this way, yellow crystals of several millimeters in length can be grown. For both modifications, crystals for X-ray diffraction and the material used in DTA/TG measurements were prepared as described above for $Nb_2O_2(SO_4)_3$. $Re_2O_7(H_2O)_2$ was prepared according to literature methods by dissolving Re metal in 30% H_2O_2 and evaporating it to dryness.[17]

2.2. X-Ray Crystallography. The selection of suitable single crystals of all four compounds was performed under inert oil. Afterward, the crystals were mounted inside an oil drop on a glass capillary (0.1 mm in diameter) and were placed into a stream of cold nitrogen (−120 °C) inside the diffractometer (IPDS I, Stoe, Darmstadt, Germany or κ-APEX II, Bruker, Karlsruhe, Germany). After checking the crystal quality and determining the unit cell parameters, the reflection intensities were collected. Table 1 presents crystallographic information for $Nb_2O_2(SO_4)_3$, $MoO_2(SO_4)$, $WO(SO_4)_2$, $Re_2O_5(SO_4)_2$−I, and $Re_2O_5(SO_4)_2$−II. Further details of the crystal structure investigations may be obtained from Fachinformationszentrum Karlsruhe, 76344 Eggenstein-Leopoldshafen, Germany (fax: (+49)7247−808−666; e-mail: crysdata@fiz-karlsruhe.de;

(6) Hayek, E.; Hinterauer, K. *Monatsh. Chem.* **1951**, *82*/*2*, 205–209.
(7) Hayek, E.; Engelbrecht, A. *Monatsh. Chem.* **1949**, *80*/*5*, 640–647.
(8) Goroshchenko, Y. G.; Andreeva, M. I. *Russ. J. Inorg. Chem.* **1965**, *10*/*4*, 517–519.
(9) Chaneliere, C.; Autran, J. L.; Devine, R. A. B.; Balland, B. *Mater. Sci. Eng.* **1998**, *22*, 269–322.
(10) Maiti, C. K.; Samanta, S. K.; Chatterjee, S.; Dalapati, G. K.; Bera, L. K. *Solid-State Electron.* **2004**, *48*, 1369–1389.
(11) Hellwig, M.; Milanov, A.; Barreca, D.; Deborde, J.-L.; Thomas, R.; Winter, M.; Kunze, U.; Fischer, R. A.; Devi, A. *Chem. Mater.* **2007**, *19*, 6077–6087.
(12) Wickleder, M. S. *Z. Anorg. Allg. Chem.* **2001**, *627*, 2112–2114.
(13) Pley, M.; Wickleder, M. S. *Z. Anorg. Allg. Chem.* **2004**, *630*, 1036–1039.
(14) Wickleder, M. S.; Büchner, O.; Gerlach, F.; Necke, M.; Al-Shamery, K.; Wich, T.; Luttermann, T. *Chem. Mater.* **2008**, *20*, 5181–5185.
(15) Wickleder, M. S. *Z. Anorg. Allg. Chem.* **2000**, *626*, 1468–1472.
(16) Hecht, H.; Jander, G.; Schlapmann, H. *Z. Anorg. Chem.* **1947**, *254*, 255–264.
(17) Brauer, G. *Handbuch der präparativen anorganischen Chemie Bd. III*; Ferdinand Enke Verlag: Stuttgart, Germany, 1981.

Table 1. Crystallographic Data for $Nb_2O_2(SO_4)_3$, $MoO_2(SO_4)$, $WO(SO_4)_2$, $Re_2O_5(SO_4)_2$−I, and $Re_2O_5(SO_4)_2$−II

chem formula	$Nb_2O_2(SO_4)_3$	$MoO_2(SO_4)$	$WO(SO_4)_2$	$Re_2O_5(SO_4)_2$	$Re_2O_5(SO_4)_2$
mol wt (g/mol)	506.00	224.00	391.97	644.52	644.52
a (Å)	9.9589(7)	8.5922(6)	7.453(1)	9.649(1)	7.1544(3)
b (Å)	11.7983(7)	12.2951(6)	11.8232(8)	8.4260(8)	7.1619(3)
c (Å)	8.6065(5)	25.671(2)	7.881(1)	5.9075(7)	16.8551(7)
β (deg)		94.567(9)	107.92(2)		
V (Å^3)	1011.3(1)	2703.4(3)	660.7(1)	480.27(9)	863.64(6)
Z	4	24	4	2	4
space group	$Pna2_1$ (No. 33)	$I2/a$ (No. 15)	$P2_1/n$ (No. 14)	$Pba2$ (No. 32)	$Pbcm$ (No. 57)
T (°C)	−120	−120	−120	−120	−120
λ (pm)	71.073	71.073	71.073	71.073	71.073
D_{calc} (g/cm^3)	3.324	3.302	3.940	4.457	4.957
μ (cm^{-1})	29.71	33.09	181.35	256.88	285.70
R_1[a]	0.0206	0.0166	0.0249	0.0322	0.0179
wR_2[b]	0.0475	0.0409	0.0556	0.0687	0.0396
Flack-X parameter	0.52(5)			0.01(2)	
CSD number	421955	421954	421958	421956	421957

[a] R_1 is defined as $\sum||F_o|-|F_c||/\sum|F_o|$ for $I > 2\sigma(I)$. [b] wR_2 is defined as $\{\sum w(F_o^2 - F_c^2)^2/\sum w(F_o^2)^2\}^{1/2}$.

Table 2. Selected Bond Lengths and Bond Angles for $Nb_2O_2(SO_4)_3$

bond lengths (pm)			
Nb1−O11	168.9(5)	Nb1−O33	198.7(3)
Nb1−O43	202.0(3)	Nb1−O44	205.5(3)
Nb1−O53	206.7(3)	Nb1−O51	229.6(4)
Nb2−O21	168.6(5)	Nb2−O34	197.3(3)
Nb2−O42	201.9(3)	Nb2−O54	202.3(3)
Nb2−O52	208.1(3)	Nb2−O32	240.6(4)
bond angles (deg)			
O11−Nb1−O33	99.3(2)	O11−Nb1−O43	96.8(2)
O11−Nb1−O44	99.0(2)	O11−Nb1−O53	98.4(2)
O21−Nb2−O34	96.9(2)	O21−Nb2−O42	100.3(2)
O21−Nb2−O52	96.7(2)	O21−Nb2−O54	98.9(2)
O11−Nb1−O51	179.7(2)	O21−Nb2−O32	179.4(2)

Table 3. Selected Bond Lengths and Bond Angles for $MoO_2(SO_4)$

bond lengths (pm)			
Mo1−O11	167.1(2)	Mo1−O12	167.8(2)
Mo1−O41	203.2(2)	Mo1−O42	204.6(2)
Mo1−O53	223.8(2)	Mo1−O43	227.7(2)
Mo2−O21	168.2(2)	Mo2−O22	167.6(2)
Mo2−O51	202.7(2)	Mo2−O61	203.6(2)
Mo2−O44	223.1(2)	Mo2−O54	228.2(2)
Mo3−O31	167.9(2)	Mo3−O32	167.6(2)
Mo3−O52	203.2(2)	Mo3−O62	205.2(2)
Mo3−O64	222.3(2)	Mo3−O63	227.1(2)
bond angles (deg)			
O11−Mo1−O12	102.3(1)	O21−Mo2−O22	102.9(1)
O31−Mo3−O32	102.88(9)	O11−Mo1−O41	98.74(8)
O12−Mo1−O42	96.01(8)	O11−Mo1−O43	167.45(9)
O12−Mo1−O53	164.83(9)	O21−Mo2−O51	99.94(8)
O22−Mo2−O61	99.02(8)	O21−Mo2−O44	164.17(9)
O22−Mo2−O54	167.97(9)	O31−Mo3−O52	98.12(8)
O32−Mo3−O62	97.82(7)	O31−Mo3−O63	168.85(7)
O32−Mo3−O64	165.42(8)		

Table 4. Selected Bond Lengths and Bond Angles for $WO(SO_4)_2$

bond lengths (pm)			
W1−O11	166.7(7)	W1−O22	200.8(7)
W1−O34	202.8(8)	W1−O33	204.9(6)
W1−O24	206.5(7)	W1−O23	206.9(6)
W1−O32	218.6(7)		
bond angles (deg)			
O11−W1−O22	93.6(3)	O11−W1−O23	97.1(3)
O11−W1−O24	95.8(3)	O11−W1−O33	99.0(3)
O11−W1−O34	97.6(3)	O11−W1−O32	176.1(3)

http://www.fiz-karlsruhe.de/request_for_deposited_data.html) on quoting the appropriate CSD number.

$Nb_2O_2(SO_4)_3$. The systematic absences suggested the orthorhombic space groups *Pnma* or $Pna2_1$. Structure solution and refinement turned out to be difficult in *Pnma*, leading to a chemically implausible structure model. However, the crystal structure could easily be solved in space group $Pna2_1$. The two niobium and three sulfur atoms were located using the direct methods of SHELXS-97;[18] the remaining oxygen atoms could be located in Fourier synthesis during the refinement with SHELXL-97.[19] A numerical absorption correction was applied to the data using the programs X-RED 1.22[20] and X-SHAPE 1.06.[21] The Flack-X parameter refined to a value of 0.52(5), so a refinement as a racemic twin was applied. Finally, the structure model refined to $R_1 = 0.0206$ for $F_o > 2\sigma(F_o)$, 0.0243 for all data, and $wR_2 = 0.0475$. Table 2 presents selected bond lengths and bond angles for $Nb_2O_2(SO_4)_3$.

$MoO_2(SO_4)$. Structure solution was achieved in the monoclinic space group $I2/a$ using the direct methods of SHELXS-97, whereas the three molybdenum and sulfur atoms as well as additional oxygen atoms could easily be located. The missing oxygen atoms were found during structure refinement in Fourier synthesis (SHELXL-97). After applying a numerical absorption correction (X-RED, X-SHAPE), the structure model refined to $R_1 = 0.0166$ for $F_o > 2\sigma(F_o)$, 0.0222 for all data, and $wR_2 = 0.0409$. Table 3 presents selected bond lengths and bond angles for $MoO_2(SO_4)$.

$WO(SO_4)_2$. The crystal structure of $WO(SO_4)_2$ could be solved in the monoclinic space group $P2_1/n$, whereas the heavy atom positions were determined using SHELXS-97—direct methods. The oxygen atoms were located during structure refinement using Fourier synthesis. A numerical absorption correction was applied to the data using X-RED and X-SHAPE. Finally, the

(18) Sheldrick, G. M. *SHELXS-97*; University of Göttingen: Göttingen, Germany, 1997.

(19) Sheldrick, G. M. *SHELXL-97*; University of Göttingen: Göttingen, Germany, 1997.

(20) *X-RED 1.22 − Data Reduction for STADI4 and IPDS*; Stoe & Cie: Darmstadt, Germany, 2001.

(21) *X-SHAPE 1.06f − Crystal Optimization for Numerical Absorption Correction*; Stoe & Cie: Darmstadt, Germany, 1999.

structure model refined to $R_1 = 0.0249$ for $F_o > 2\sigma(F_o)$, 0.0511 for all data, and $wR_2 = 0.0556$. Table 4 presents selected bond lengths and bond angles for $WO(SO_4)_2$.

$Re_2O_5(SO_4)_2$−I. The systematic absences suggested either the orthorhombic space group *Pbam* or *Pba*2. Structure solution and refinement in *Pbam* failed to result in a chemically plausible structure model. Hence, the crystal structure was solved in space group *Pba*2 using the direct methods of SHELXS-97. Only the rhenium atom could be located; the positions of the remaining sulfur and oxygen atoms were determined during structure refinement in Fourier synthesis. After applying a numerical absorption correction, the structure model converged to $R_1 = 0.0322$ for $F_o > 2\sigma(F_o)$, 0.0365 for all data, and $wR_2 = 0.0687$. The correct absolute structure is indicated through the Flack-X parameter of 0.01(2). Table 5 presents selected bond lengths and bond angles for $Re_2O_5(SO_4)_2$−I.

$Re_2O_5(SO_4)_2$−II. Initially, the metric of the unit cell suggested a tetragonal setting with the *a* and *b* axes being almost equal. But after the integration of the data set, the R_{int} value was very high (45%); furthermore, no systematic absences fitting to any tetragonal space group could be found. For this reason, the unit cell determination and integration was repeated, leading to a primitive orthorhombic unit cell. Systematic absences were easily fulfilled for the centrosymmetric space group *Pbcm*. Structure solution and refinement using the SHELXS/SHELXL programs were uncomplicated. After applying a numerical absorption correction using X-RED and X-SHAPE, the structure model converged to $R_1 = 0.0179$ for $F_o > 2\sigma(F_o)$, 0.0190 for all data, and $wR_2 = 0.0396$. Table 6 presents selected bond lengths and bond angles for $Re_2O_5(SO_4)_2$−II.

Table 5. Selected Bond Lengths and Bond Angles for $Re_2O_5(SO_4)_2$−I

bond lengths (pm)			
Re1−O11	167(1)	Re−O12	169(1)
Re1−O13	188.3(3)	Re1−O24	195(1)
Re1−O23	215.9(9)	Re1−O22	218.8(9)
bond angles (deg)			
O11−Re1−O12	103.8(5)	Re1−O13−Re1	149.2(7)
O11−Re1−O24	93.6(5)	O12−Re1−O13	97.5(4)
O11−Re1−O22	165.6(5)	O12−Re1−O23	167.4(4)

Table 6. Selected Bond Lengths and Bond Angles for $Re_2O_5(SO_4)_2$−II

bond lengths (pm)			
Re1−O11	167.7(4)	Re1−O12	168.7(4)
Re1−O13	186.55(9)	Re1−O33	191.9(4)
Re1−O22	215.8(3)	Re1−O21	220.7(4)
bond angles (deg)			
O11−Re1−O12	102.4(2)	Re1−O13−Re1	161.4(3)
O11−Re1−O33	96.6(2)	O12−Re1−O13	96.6(2)
O11−Re1−O21	170.3(2)	O12−Re1−O22	167.4(2)

2.3. Thermal Analysis. The investigation of the thermal behavior was performed using a TGA/SDTA apparatus (TGA/SDTA851^e, Mettler-Toledo GmbH, Schwerzenbach, Switzerland). In a flow of dry nitrogen, 10−20 mg of the compound was placed in a corundum crucible and heated at a rate of 10 K/min up to 1050 °C. The collected data were processed using the software of the analyzer (Mettler-Toledo STAR^e V8.1).[22] Thermal decomposition data for $Nb_2O_2(SO_4)_3$, $MoO_2(SO_4)$, $WO(SO_4)_2$, $Re_2O_5(SO_4)_2$−I, and $Re_2O_5(SO_4)_2$−II are presented in Table 7.

2.4. X-Ray Powder Diffraction. The residues after the thermal decomposition of $Nb_2O_2(SO_4)_3$ and $WO(SO_4)_2$ have been characterized by means of powder diffraction with a STADI P powder diffractometer (Stoe, Darmstadt, Germany) using Cu Kα radiation. The diffraction data were processed with the WinXPow 2007 program package (Stoe, V. 2.20).[23]

3. Results and Discussion

3.1. Crystal Structures. $Nb_2O_2(SO_4)_3$ crystallizes orthorhombically with space group $Pna2_1$ and contains four formula units in the unit cell. The two crystallographically different niobium atoms are in a distorted octahedral coordination of five monodentate sulfate ions and one oxide ligand (Figure 1). The distances to the oxide ions (O11, O21) are about 169 pm in both octahedra, which is usually

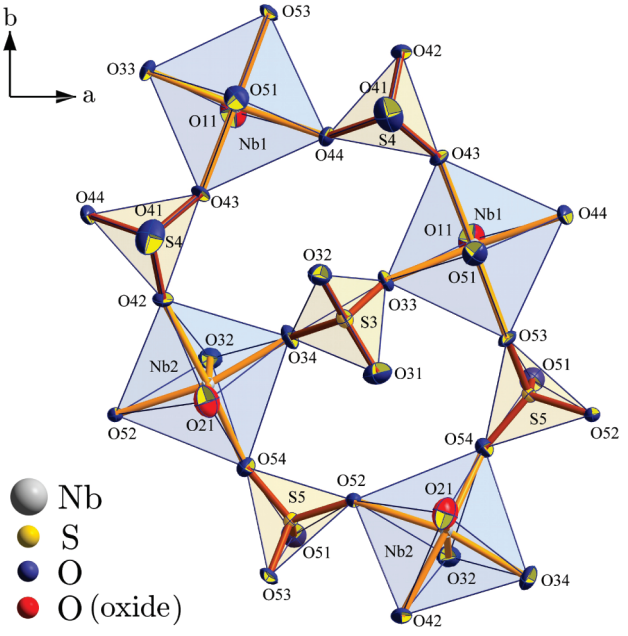

Figure 1. Atom labeling scheme and thermal ellipsoids drawn at 75% probability for $Nb_2O_2(SO_4)_3$. Four [Nb═O] units are connected through four [SO_4] tetrahedra to eight-membered rings, which are centered by an additional sulfate group. For both crystallographically distuingishable Nb atoms, a distorted octahedral coordination results.

Table 7. Thermal Decomposition Data for for $Nb_2O_2(SO_4)_3$, $MoO_2(SO_4)$, $WO(SO_4)_2$, $Re_2O_5(SO_4)_2$−I, and $Re_2O_5(SO_4)_2$−II

compound	step	T_S (°C)	T_{max} (°C)	T_E (°C)	reaction/product	Δm_{exp} (%)	Δm_{calc} (%)
$Nb_2O_2(SO_4)_3$	1	650	697	750	$-3SO_3/Nb_2O_5$	48.1	47.5
$MoO_2(SO_4)$	1	400	490	540	$-SO_3/MoO_3$	36.3	35.8
	2	775	792	805	melting of MoO_3		
$WO(SO_4)_2$	1	270	326		$1-3\} - 2SO_3/WO_3$	45.1	40.8
	2		425				
	3		515	530			
$Re_2O_5(SO_4)_2$−I	1	206	242		$1-2\} - 2SO_3/Re_2O_7\uparrow$	99.9	100
	2		306	335			
$Re_2O_5(SO_4)_2$−II	1	206	233	260	$-SO_3/Re_2O_6(SO_4)$	12.2	12.4
	2	270	341	365	$-SO_3/Re_2O_7\uparrow$	98.9	100

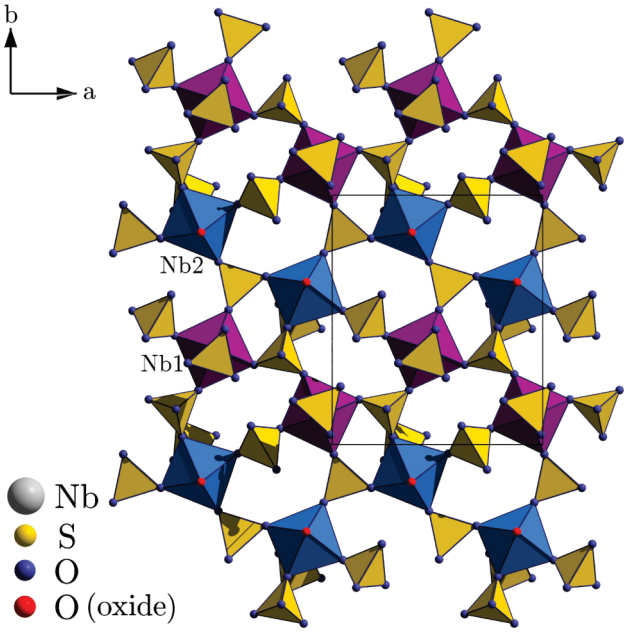

Figure 2. Layers parallel to (001) in $Nb_2O_2(SO_4)_3$ built by sulfate-centered eight-membered rings of four [Nb=O] moieties and four sulfate tetrahedra. Along [100], zigzag chains containing either [Nb1=O] (violet) or [Nb2=O] moieties (blue) are formed.

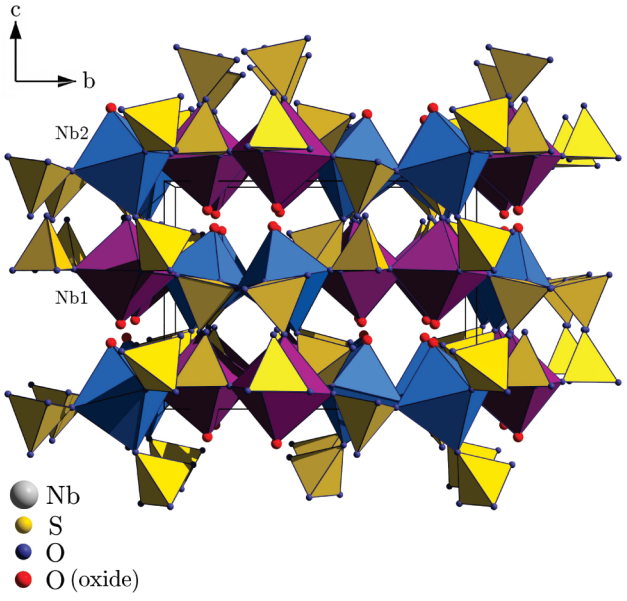

Figure 3. Layers in $Nb_2O_2(SO_4)_3$ parallel to (001) connected to a three-dimensional network, which is pervaded by channels along [100], inside which the [Nb=O] moieties are aligned. The arrangement of the [Nb1=O] (violet) and [Nb2=O] zigzag chains (blue) alternates in both the [010] and [001] directions.

interpreted as a Nb=O double bond. The Nb−O distances *trans* to the oxide ligands are the longest within the octahedra and have lengths of 230 and 241 pm, respectively. The remaining four Nb−O distances range from 197 to 208 pm in both coordination polyhedra. The niobium atom inside the $[Nb1O_6]$ as well as the $[Nb2O_6]$ octahedron is clearly displaced toward the vertex of the polyhedron formed by the terminal oxide ligand, easily reflected in the angles O_{oxide}−Nb−$(OSO_3)_{cis}$ ranging between 97 and 100°.

There are three crystallographically different sulfate ions represented by the sulfur atoms S3, S4, and S5. The sulfate tetrahedra are attached to three (S3, S4) and four (S5) niobium atoms, so that the connectivity can be described by $[NbO(SO_4)_{3/3}(SO_4)_{2/4}]$ according to Niggli's formalism. The S−O distances within the anions reflect the different coordinations of the oxygen atoms. Those which are not bonded to a Nb atom (O31, O41) show short bond lengths around 141 pm, while the remaining S−O distances range from 146 up to 153 pm. As can be seen from Figure 2, all sulfate ions connect the niobium atoms within the (001) plane to layers. These layers are built up by octagonal alternating arrangements of four sulfate tetrahedra (S4, S5) and four niobium atoms, whereas an additional sulfate group (S3) inside the octagon connects two opposing niobium atoms.

Additionally, two of the three crystallographically different sulfate anions (S3, S5) take care for the linkage of the layers in the [001] direction (bonds Nb1−O51 and Nb2−O32 in Figure 1). This connection is realized exclusively through the weaker Nb−$(OSO_3)_{trans}$ bonds. Within this three-dimensional network, zigzag chains in the [100] direction assembled by only one of the crystallographically different niobium atoms Nb1 or Nb2 are shaped (Figure 3). In both the [010] and [001] directions, the sequence of these zigzag chains is alternating Nb1 and Nb2. The crystal structure is also pervaded by channels in the [100] direction, inside which the [Nb=O] moieties are oriented. Thereby, it is important to mention that the [Nb1=O] units are always aligned in the [00−1] direction and the [Nb2=O] groups always toward [001].

Generally, a Flack-X parameter of around 0.5 indicates a racemic twinning of the crystal. However, as is often a warning sign of an overlooked inversion center, the crystal structure of $Nb_2O_2(SO_4)_3$ has been searched for a center of symmetry, which would result in the centrosymmetric space group *Pnma* and would render Nb1 and Nb2 as well as two of the sulfate tetrahedra crystallographically equal. There seem possible locations for a center of symmetry in the middle of the 8-fold rings of [Nb=O] moieties and $[SO_4]$ tetrahedra in the layers parallel to the (001) plane or within the channels along [100] formed by the terminal oxide ligands. In both cases, the heavier atoms are able to fulfill additional inversion symmetry, but it is clearly penetrated at least by the oxygen atoms. This is easily reflected in the significantly different coordination sphere around Nb1 and Nb2, as the bond to the sulfate ligand in the *trans* position differs by about 11 pm in length, for example. Therefore, the structure is best described without any inversion symmetry, and the acentric space group $Pna2_1$ is a reasonable choice here. However, the Flack-X parameter indicates that the energetic difference between the two orientations of a layer inside the crystal structure is rather low. Hence, on a macroscopic scale, the crystal contains both orientations in a statistic distribution according to a racemic twinning, which is represented in the Flack-X parameter.

$MoO_2(SO_4)$ crystallizes in the monoclinic space group $I2/a$ with 24 formula units in the unit cell. Resulting in a smaller monoclinic angle, the space group $I2/a$ has been preferred over the *C*-centered setting. Except for the different cell choice, the crystal structure is in accord with

(22) *STAR*^{e}; Mettler−Toledo GmbH: Schwerzenbach, Switzerland, 2004.
(23) *WinXPOW 2007*; Stoe & Cie: Darmstadt, Germany, 2006.

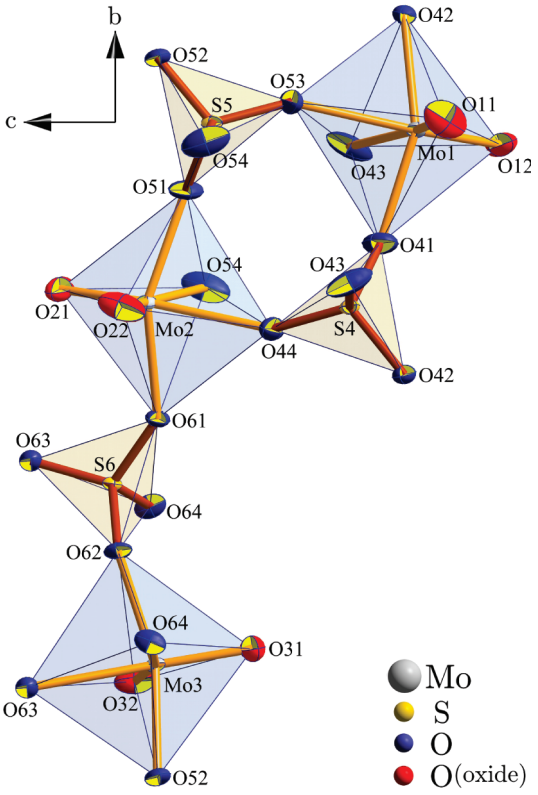

Figure 4. Atom labeling scheme and thermal ellipsoids drawn at 75% probability for $MoO_2(SO_4)$. The three crystallographically different Mo atoms are in distorted octahedral coordination of two terminal oxide ligands and four sulfate tetrahedra.

the results published by Christansen et al. for the monoclinic modification of $MoO_2(SO_4)$.[3] The asymmetric unit of $MoO_2(SO_4)$ contains three crystallographically distinguishable molybdenum atoms, which are each in a distorted octahedral coordination of two terminal oxide ligands and four monodentate sulfate ions (Figure 4). The distances to the terminal oxygen atoms (O11, O12, O21, O22, O31, O32) are short, ranging between 167 and 168 pm. The oxide ligands in the "molybdenyl" group are arranged in *cis* orientation to each other, with an O−Mo−O angle of 103°. This is quite typical for high valent transition metals—in contrast to the well-known linear $[O{=}An{=}O]^{n+}$ units formed by the actinide elements.[24,25] All three crystallographically distinguishable $[MoO_6]$ octahedra are significantly distorted; the Mo atom inside each polyhedron is considerably displaced toward the edge of the octahedron formed by both terminal oxide ligands, clearly visible in the $O_{oxide}-Mo-(OSO_3)_{cis}$ angles ranging between 96 and 100°. The Mo−O distances to the sulfate ions in the *cis* position toward the terminal oxide ligands are inconspicuous, ranging between 203 and 205 pm. As expected, the longest bonds within each octahedron are the Mo−O distances *trans* to the Mo=O groups (222−229 pm). Interestingly, the elongation of the Mo−O bonds *trans* to the oxide ligands is around 10 pm smaller than in $Nb_2O_2(SO_4)_3$; probably, the higher charge of Mo compared to Nb plays an essential role here.

(24) Denning, R. G. *J. Phys. Chem. A* **2007**, *111*, 4125–4143.
(25) Müller, K.; Foerstendorf, H.; Tsushima, S.; Brendler, V.; Bernhard, G. *J. Phys. Chem. A* **2009**, *113*, 6626–632.

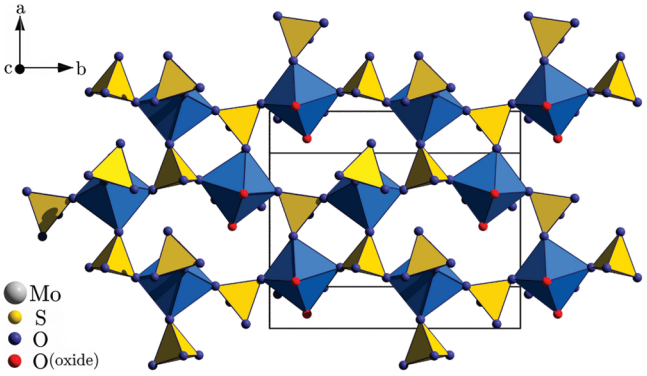

Figure 5. Layers parallel to (001) in $MoO_2(SO_4)$ built by eight-membered rings of four $[MoO_2]$ units and four sulfate tetrahedra. One of the terminal oxide ligands on each Mo atom is aligned toward the center of such a ring; the other is oriented perpendicular on the layer toward [001] or [00−1].

Three crystallographically different sulfate tetrahedra, represented by the sulfur atoms S4, S5, and S6, are located within the asymmetric unit. All of them are attached to four different molybdenum atoms, so that the connectivity can be described as $[MoO_2(SO_4)_{4/4}]$ according to Niggli's formalism. Each sulfate group connects two $[MoO_2]$ moieties, so chains along [010] are formed. The coordination to these Mo atoms is always realized in the *cis* position to the Mo=O groups. A third $[SO_4]$ oxygen atom, which is not involved in building these chains, takes care of their linkage to each other in the [100] direction. This connection is exclusively realized by coordination in the *trans* position to the Mo=O groups of the neighboring chains. In this way, layers parallel to the (001) plane are formed (Figure 5). Within the layers, the arrangement of the oxide ligands on the Mo atoms leads to the development of 8-fold rings built by four $[MoO_2]$ moieties as well as four sulfate tetrahedra. One oxide ligand on each molybdenum atom is aligned toward the center of such an 8-fold ring; the second one sticks out of the layers in the [001] or [00−1] direction. As can be seen from Figure 6, the crystal structure consists of three different types of these layers: one contains only $[Mo1O_6]$ octahedra (A), whereas the others both embody $[Mo2O_6]$ as well as $[Mo3O_6]$ (B,C). Finally, the fourth oxygen atom on each sulfate tetrahedron connects these layers along [001] to a three-dimensional network. The crystal structure of $MoO_2(SO_4)$ is pervaded by channels along [100], inside which one-half of the oxide ligands are oriented. The layers are packed along [001] according to the schemes B, A, C, *glide plane*, C*, A*, B* , etc., whereas the layers A/A*, B/B*, and C/C* are transformed into each other by glide planes located at $z = 0$, 0.5, and 1.

$WO(SO_4)_2$ crystallizes in the monoclinic space group $P2_1/n$ and contains four formula units in the unit cell. In contrast to the other compounds, the only crystallographically independent tungsten atom in the asymmetric unit of $WO(SO_4)_2$ is in pentagonal bipyramidal coordination with one terminal oxide ligand and two monodentate and two bidentate sulfate ions (Figure 7). For a d^0 system like W^{VI}, which has no explicit preference for octahedral coordination due to ligand field effects, a 7-fold coordination is not surprising. As expected, the distance to the terminal oxide ligand (O11) is short with 167 pm.

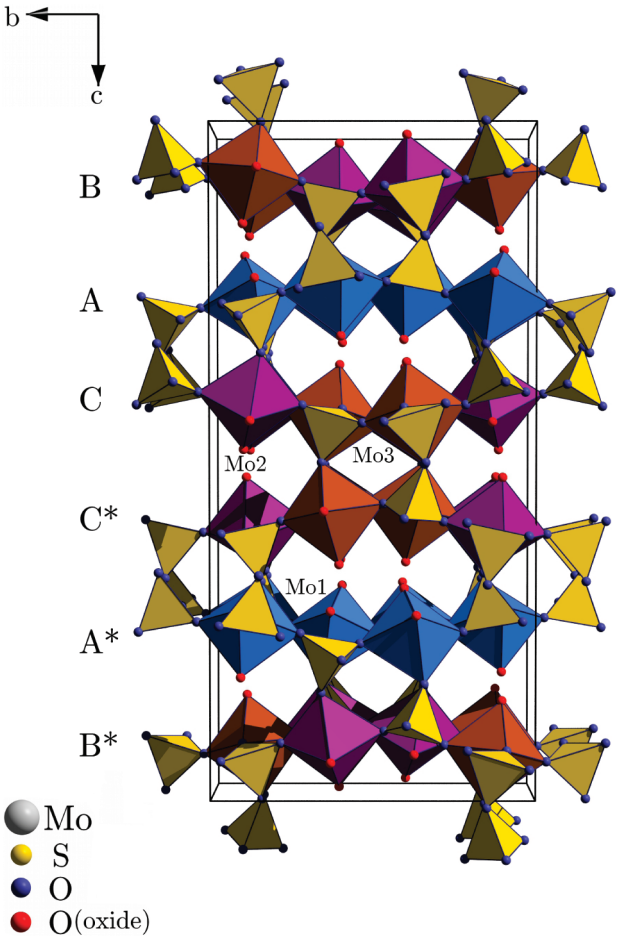

Figure 6. The three different types of layers (A, B, C) in $MoO_2(SO_4)$ connected to a three-dimensional network. Layers of type A contain only $[Mo1O_2]$ units (blue), whereas B and C are built by both $[Mo2O_2]$ (violet) and $[Mo3O_2]$ (brown). The layers A*, B*, and C* are generated by glide planes located at $z = 0$, 0.5, and 1. Along [100], channels are formed, which accommodate one-half of the terminal oxide ligands on each Mo atom.

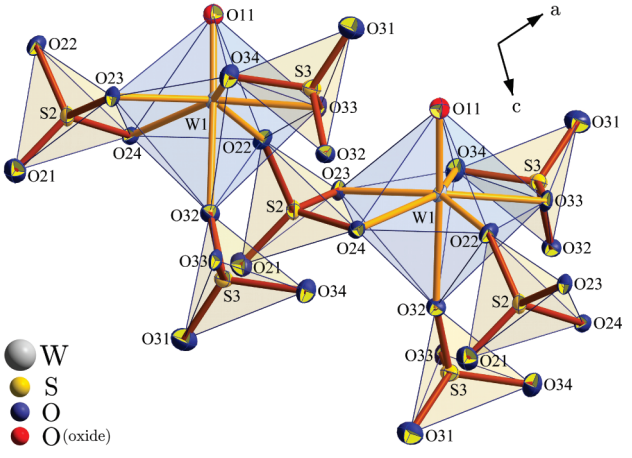

Figure 7. Atom labeling scheme and thermal ellipsoids drawn at a 50% probability level for $WO(SO_4)_2$. The tungsten atom is in distorted pentagonal bipyramidal coordination with one terminal oxide ligand and two monodentate and two bidentate sulfate anions.

In the *trans* position thereto, a monodentate sulfate group [O32SO$_3$] coordinates to the tungsten atom at a distance of 219 pm. The elongation of this W−$(OSO_3)_{trans}$ bond is comparable to the values found for $MoO_2(SO_4)$. The pentagonal bipyramid around tungsten is completed by two bidentate sulfate ions [O23−SO_2−O24] and [O33−SO_2−O34], respectively, as well as a second monodentate sulfate group [O22−SO_3] in a position *cis* to the [W=O] unit. These W−O distances range between 201 and 207 pm. The tungsten atom is displaced toward the vertex of the pentagonal bipyramid formed by the terminal oxide ligand, easily reflected in the widened angles O_{oxide}−W−$(OSO_3)_{cis}$ with values between 94 and 99°.

The asymmetric unit contains two crystallographically different sulfate ions represented by the sulfur atoms S2 and S3. Each sulfate group coordinates two different tungsten atoms, one of them as a chelating ligand utilizing two oxygen atoms, the other as a monodentate ligand. One oxygen atom of each sulfate ion does not coordinate at all (O21, O31), which is clearly represented in the short S−O distance of 140 pm. According to Niggli's formalism, the connectivity in $WO(SO_4)_2$ can be described as $[WO(SO_4)_{4/2}]$. The difference between both sulfate tetrahedra is their behavior as monodentate ligands: [S3O$_4$] coordinates the tungsten atom in a *trans* position to the [W=O] unit; [S2O$_4$] to the contrary tethers the W atom *cis* to the oxide ligand. This leads to slightly different S−O distances (S2−O22, 150 pm; S3−O32, 148 pm), due to the weaker W−O32 bond. The longest S−O distances inside the sulfate tetrahedra are the bonds to the oxygen atoms which are employed for the chelating coordination of tungsten (O23, O24, O33, and O34) ranging between 152 and 154 pm. Both sulfate tetrahedra are strongly distorted; due to the bidentate coordination of tungsten, the O23−S2−O24 and O33−S3−O34 angles (95 and 97°, respectively) are clearly below the ideal tetrahedral angle.

Finally, the sulfate ions connect the [W=O] units forming corrugated layers which run parallel to the (10−1) plane (Figure 8). These layers are built from rings composed of six [W=O] moieties as well as six [SO$_4$] tetrahedra, whereas each ring embodies a center of symmetry in the middle. The terminal oxide ligands and the noncoordinating sulfate oxygen atoms are aligned perpendicularly toward these layers and stick out in the [−101] and [10−1] directions, respectively. Viewed along [101], zigzag chains with the [W=O] groups placed alternatingly on the top and the bottom of the layers are formed. The cohesion between two layers in the crystal structure is realized through weaker W−O contacts (W−O dist. 380 pm) between the noncoordinating [SO$_4$] oxygen atoms of one layer and the tungsten atoms from the layer above and below (Figure 9).

$Re_2O_5(SO_4)_2$−I crystallizes in the orthorhombic space group *Pba*2 with two formula units per unit cell. The asymmetric unit contains only one rhenium atom, which is in distorted octahedral coordination with two terminal oxide ligands, one bridging oxygen atom, and three monodentate sulfate ions (Figure 10). The distances to the terminal oxide ligands (O11, O12) with values of 167 and 169 pm are short, as expected; the oxide ligands are aligned in a position *cis* to each other. Two of these [ReO_2] units are connected by an additional oxide ligand (O13), which is located on a special site of the space group *Pba*2 (2*b*, 2-fold axis), so finally a [Re_2O_5] group (Re−O−Re angle: 149°) with a staggered conformation of the [ReO_2] units is formed (O11−Re1−Re1−O12 torsion

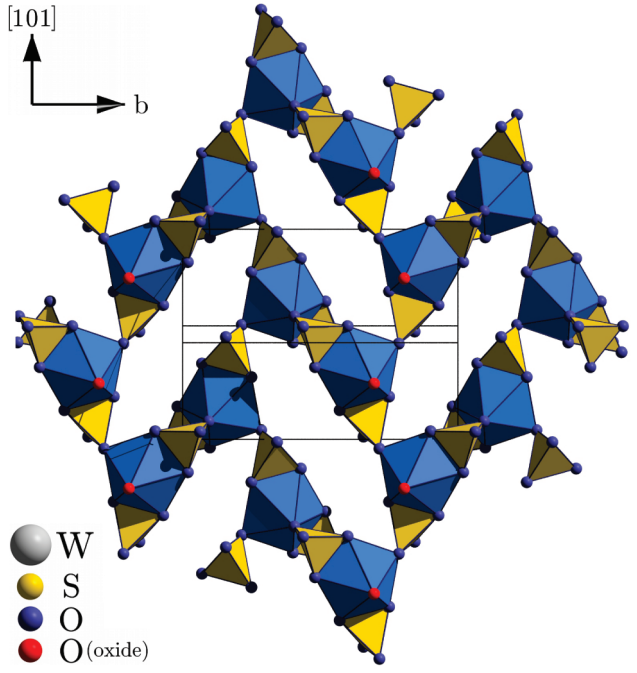

Figure 8. [W=O] moieties in $WO(SO_4)_2$ connected by $[SO_4]$ tetrahedra to layers parallel to (10−1). The terminal oxide ligands on each W atom and the noncoordinating $[SO_4]$ oxygen atoms, however, stick out of these layers toward [10−1] and [−101].

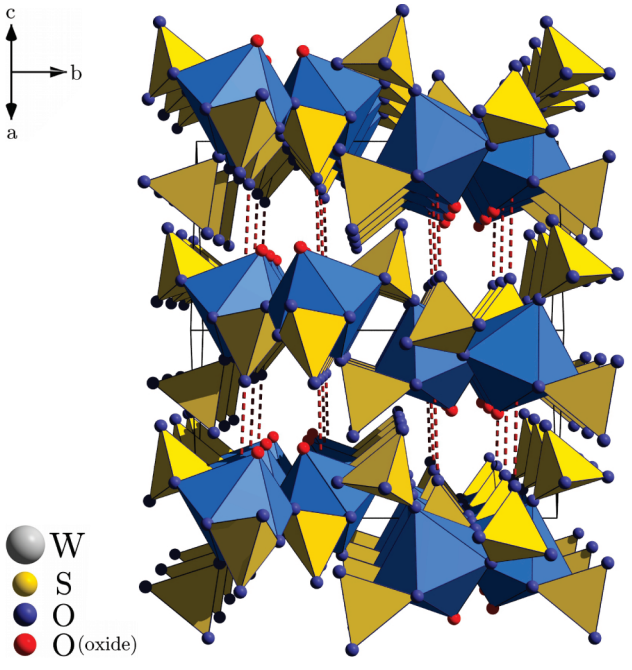

Figure 9. Layers built by [W=O] moieties and sulfate tetrahedra packed loosely on top of each other in the [10−1] direction. The cohesion between two layers is realized through weak W−O contacts (380 pm, dashed bonds).

angle: 23°). Additionally, each $[Re_2O_5]$ group is coordinated by four sulfate tetrahedra, completing the octahedral coordination of each Re atom.

The $[ReO_6]$ polyhedra in $Re_2O_5(SO_4)_2$−I are significantly distorted; the Re atom is displaced toward the edge of the octahedron formed by the terminal oxide ligands. This is clearly represented in the elongation of the bonds to the ligands *trans* to Re=O (dist. Re−O22SO_3: 219 pm;

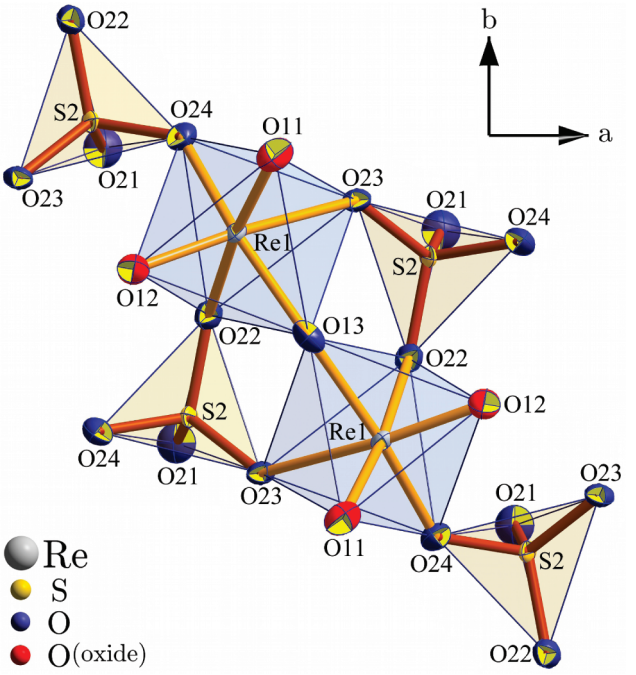

Figure 10. Atom labeling scheme and thermal ellipsoids drawn at a 75% level for $Re_2O_5(SO_4)_2$−I. Each Re atom is in distorted octahedral coordination with two terminal oxide ligands, three sulfate ions, and one bridging oxygen atom. In the $[Re_2O_5]$ unit formed, both $[ReO_2]$ moieties are tilted only slightly.

dist. Re−O23SO_3: 216 pm) and the O_{oxide}−Re−$(OSO_3)_{cis}$ and O_{oxide}−Re−O_{bridge} angles ranging between 94 and 99°. Obviously, the higher charge of the metal leads again to slightly less elongation of the bonds to the ligands *trans* to the Re=O groups compared to the niobium, molybdenum, and tungsten compound.

The S2 sulfur atom represents the only sulfate ion in the asymmetric unit. Altogether, it coordinates three different rhenium atoms, whereas two of them belong to the same $[Re_2O_5]$ group and the third to a neigbouring one. One oxygen atom of the sulfate tetrahedron (O21) does not coordinate at all, clearly visible by the short S−O distance of 141 pm. The connectivity in $Re_2O_5(SO_4)_2$−I can be described as $[(ReO_2)O_{1/2}(SO_4)_{3/3}]$ according to Niggli's formalism. The other S−O bond lengths inside the tetrahedron evince very clearly, whether the coordination to the metal takes place in the *trans* position (S−O22/23 dist.: 149 pm) or the *cis* position toward the Re=O group (S−O24 dist.: 155 pm).

Finally, the linkage of the $[Re_2O_5]$ units by the sulfate ions results in layers parallel to the (001) plane (Figure 11). These layers have a remote relationship to the ones formed in $MoO_2(SO_4)$. Both contain 8-fold rings in the midst of which M=O groups are aligned. Their chief difference is, on the one hand, the condensation of two $[MO_6]$ octahedra to dimers in $Re_2O_5(SO_4)_2$−I and, on the other hand, the alignment of the terminal oxide ligands in the [001] direction. In $Re_2O_5(SO_4)_2$−I, the terminal oxide ligands all point toward [001], whereas the noncoordinating oxygen atoms on the sulfate ions are oriented the other way around along [00−1]. Viewed along the crystallographic *b* axis, the layers in $Re_2O_5(SO_4)_2$−I can be described as a layer of $[Re_2O_5]$ units with their terminal oxide ligands aligned on top, whereas the $[Re_2O_5]$ moieties

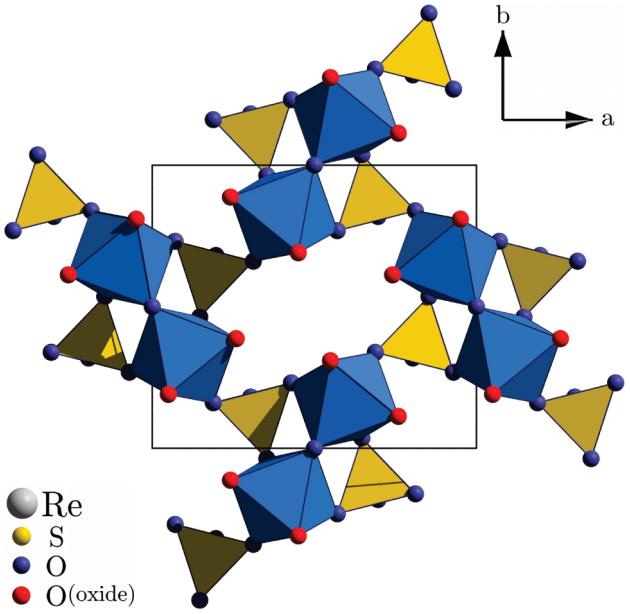

Figure 11. $[Re_2O_5]$ moieties in $Re_2O_5(SO_4)_2$−I connected through sulfate ions to layers which run parallel to the (001) plane. They contain 8-fold rings of four $[ReO_2]$ units and four sulfate tetrahedra similar to $MoO_2(SO_4)$.

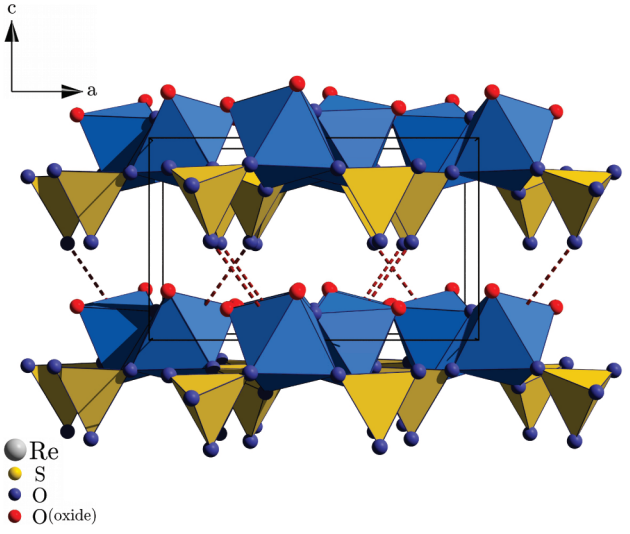

Figure 12. Layers built by $[Re_2O_5]$ units and $[SO_4]$ tetrahedra in $Re_2O_5(SO_4)_2$−I packed directly one upon another. On top of a layer, the terminal oxide ligands of each Re atom are aligned, whereas the noncoordinating $[SO_4]$ oxygen atoms stick out in the opposite direction. The shortest distance Re−O between two layers is 343 pm (dashed bonds).

are connected through sulfate ions with one noncoordinating oxygen atom on the bottom (Figure 12). In the crystal structure, these layers are packed only loosely one upon another along [001]. The cohesion between two layers is realized through weaker Re−O interactions (Re−O dist.: 343 pm) between the noncoordinating $[SO_4]$ oxygen atoms and the rhenium atoms from the layer beneath.

$Re_2O_5(SO_4)_2$−II crystallizes in the orthorhombic space group *Pbcm* with four formula units in the unit cell. The asymmetric unit contains one rhenium atom, which is in distorted octahedral coordination of two terminal oxide ligands, one bridging oxygen atom, and three monodentate sulfate ions (Figure 13). The terminal oxide ligands

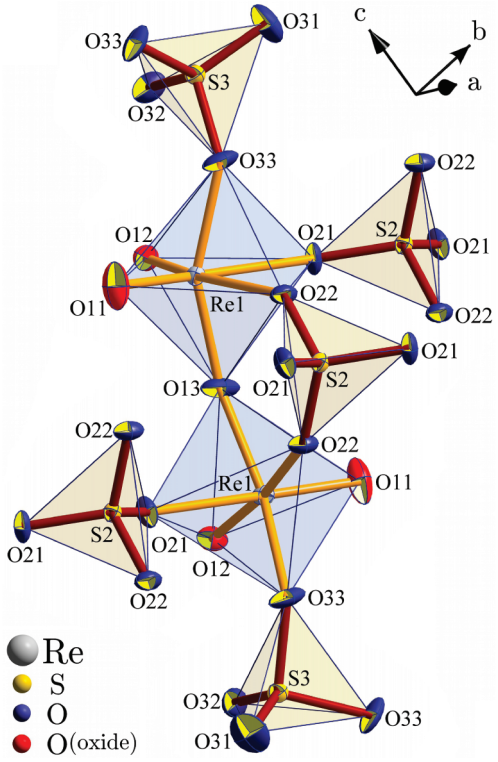

Figure 13. Atom labeling scheme and thermal ellipsoids drawn at a 75% probability level for $Re_2O_5(SO_4)_2$−II. Each Re atom is in distorted octahedral coordination with two terminal oxide ligands, one bridging oxygen atom, and three sulfate ions. In the $[Re_2O_5]$ unit formed, the tilt of the $[ReO_2]$ moieties is much more pronounced than in $Re_2O_5(SO_4)_2$−I.

(O11, O12) are in orientation *cis* to each other. As expected, the Re=O distances are short at 168 and 169 pm, whereas the distance to the ligands in the *trans* position is significantly widened (216 and 221 pm). Analogous to $Re_2O_5(SO_4)_2$−I, two $[ReO_2]$ groups are connected to a $[Re_2O_5]$ moiety by a bridging oxygen atom (Re−O−Re angle, 161°; Re−O dist., 187 pm), which is located on a special site of the space group *Pbcm* (4*c*, 2-fold axis). A minor difference between the two modifications of $Re_2O_5(SO_4)_2$ is the tilt between both $[ReO_2]$ units with a O11−Re1−Re1−O12 torsion angle of only 23° found in $Re_2O_5(SO_4)_2$−I but 93° in $Re_2O_5(SO_4)_2$−II. A major difference is the coordination of the $[Re_2O_5]$ unit by the sulfate ions. In $Re_2O_5(SO_4)_2$−II, each $[Re_2O_5]$ group is coordinated by one chelating and four monodentate $[SO_4]$ tetrahedra, whereas in $Re_2O_5(SO_4)_2$−I, the $[Re_2O_5]$ unit is bonded by two monodentate and two chelating sulfate ions. This is a direct consequence of the larger tilt between the $[ReO_2]$ groups. In $Re_2O_5(SO_4)_2$−II, only two free coordination places on the $[Re_2O_5]$ unit come close enough together, so that a chelating attack of a sulfate ligand is possible. Like in $Re_2O_5(SO_4)_2$−I, the $[ReO_6]$ polyhedron is visibly distorted with the metal atom displaced toward the edge of the octahedron formed by both terminal oxide ligands (O_{oxide}−Re−$(OSO_3)_{cis}$ and O_{oxide}−Re−O_{bridge} angles ranging between 97 and 100°).

The asymmetric unit of $Re_2O_5(SO_4)_2$−II contains two crystallographically distinguishable sulfate ions. $[S2O_4]$ is located on a 2-fold axis (site 4*c*) and coordinates with all four oxygen atoms to four different rhenium atoms. $[S3O_4]$ sits on a mirror plane (site 4*d*) and connects only

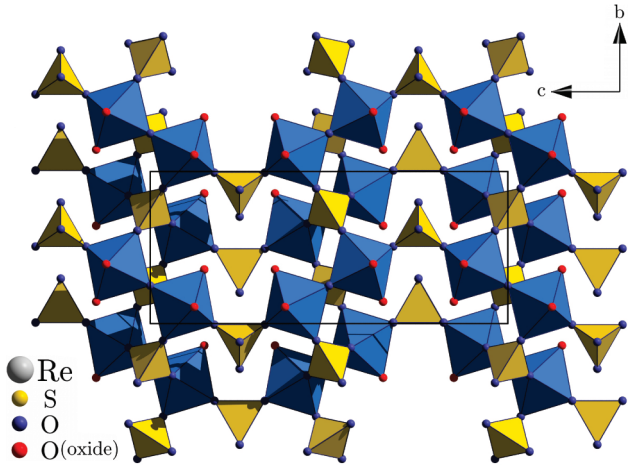

Figure 14. $[Re_2O_5]$ units in $Re_2O_5(SO_4)_2$−II connected through $[SO_4]$ tetrahedra in the [001] direction to zigzag chains. Each bend of these chains is represented by a mirror plane at $z = 0.25$ and 0.75. Additionally, two chains are connected along [100], so finally double layers are formed. On both sides of the double layer, the terminal oxide ligands on the Re atoms and the noncoordinating $[SO_4]$ oxygen atoms stick out in the [100] and [−100] directions, respectively.

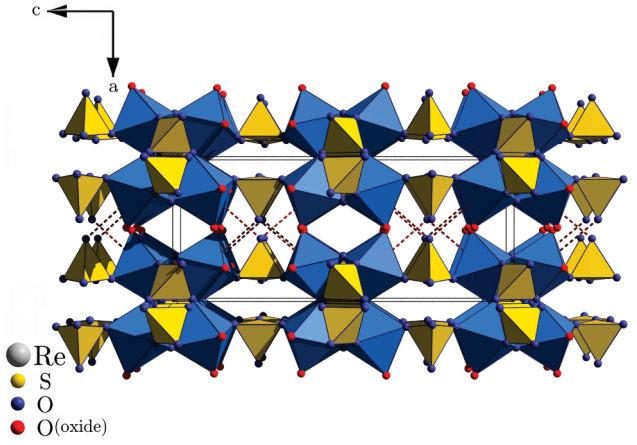

Figure 15. Double layers in $Re_2O_5(SO_4)_2$−II built by the connection of $[Re_2O_5]$ units through $[SO_4]$, packed directly one upon another in the [100] direction. The cohesion between two layers is realized through weak Re−O interactions between the noncoordinating $[SO_4]$ oxygen atoms and the Re atoms of the neighboring layers.

two Re atoms and leaves two oxygen atoms uncoordinated. This behavior is clearly represented in the S−O distances, which are almost equal for S2−O21/22 at 146 and 147 pm but differ largely for $[S3O_4]$ between the noncoordinating S−O groups (S3−O31/32: 141 and 142 pm) and the coordinating ones (S3−O33: 156 pm). According to Niggli's formalism, the connectivity in $Re_2O_5(SO_4)_2$−II can be described as $[(ReO_2)O_{1/2}(SO_4)_{1/2}(SO_4)_{2/4}]$. The $[Re_2O_5]$ units are connected through $[S3O_4]$ tetrahedra to zigzag chains in the [001] direction, whereas the sulfate ions always coordinate in the *trans* position toward the Re−O−Re bridge (Figure 14). Each bend of these zigzag chains is represented by a mirror plane which is located parallel to the (001) plane at $z = 0.25$ and 0.75.

$[S2O_4]$ takes care of the linkage of these chains in both the [100] and [010] directions. Altogether, each $[S2O_4]$ tetrahedron connects three different chains, at first two of them in the [010] direction, whereas the sulfate ion acts as a monodentate ligand toward both $[Re_2O_5]$ units. The two residual oxygen atoms of the $[S2O_4]$ tetrahedron tether a third chain in the [100] direction. Here, the sulfate ion acts as a chelating ligand toward the $[Re_2O_5]$ moiety. In all cases, the bonding of $[S2O_4]$ takes place in the *trans* position toward a Re=O group, which explains the significantly shorter S−O distances compared to the ones found for $[S3O_4]$. The linkage of the chains along [100] does not take place indefinitely. Only two chains are connected to each other, so double layers parallel to (001) are formed (Figure 15).

Finally, the crystal structure of $Re_2O_5(SO_4)_2$−II is built by stacking these double layers in the [100] direction. On both sides of each double layer, the terminal oxide ligands on the Re atoms and the noncoordinating oxygen atoms of the sulfate groups point out toward [100] and [−100] (Figure 15). Between two layers, only weaker interactions between the Re atoms with the sulfate tetrahedra of the neighboring layer take place (Re−O dist.: 368 pm).

3.2. Thermal Decomposition. The thermal decomposition of $Nb_2O_2(SO_4)_3$ follows a one-step mechanism and leads after an endothermic loss of three SO_3 molecules per formula unit to Nb_2O_5. The decomposition product has been analyzed by means of X-ray powder diffraction and could be identified as the monoclinc high temperature modification of niobium pentoxide (*H*-Nb_2O_5) reported by Kato.[26] The crystallinity of the decomposition residue is low, which is visible from the broadened reflections in the powder pattern. Despite its relatively high sulfate content, the thermal stability of $Nb_2O_2(SO_4)_3$ is astonishingly high. The decomposition starts at 650 °C and is complete at 750 °C with a maximum at 697 °C. The decomposition temperature of $Nb_2O_2(SO_4)_3$ is comparable to the findings of Boström et al. for $Nb_2O_3(SO_4)_2 \cdot 0.25H_2O$, which degrades between 500 and 800 °C to Nb_2O_5.[5] The similar thermal stability of $Nb_2O_2(SO_4)_3$ and $Nb_2O_3(SO_4)_2 \cdot 0.25H_2O$ explains the one step decomposition mechanism of $Nb_2O_2(SO_4)_3$, which probably loses one SO_3 molecule under the intermediate formation of $Nb_2O_3(SO_4)_2$. The latter is not stable under these conditions and gives off the remaining SO_3 molecules immediately, forming Nb_2O_5.

$MoO_2(SO_4)$ decomposes at considerably lower temperatures than $Nb_2O_2(SO_4)_3$. The decomposition proceeds in a single endothermic step beginning at 400 °C and ending at 540 °C with a peak maximum at 490 °C. With respect to the observed loss of mass, the decomposition is in accord with the loss of one SO_3 molecule per formula unit, forming MoO_3 as a product. A second endothermic peak in the DTA curve between 775 and 805 °C (max. 792 °C) can be interpreted as the melting of MoO_3 (mp 795 °C).[27] Finally, further heating leads to the complete sublimation of MoO_3.

The thermal treatment of $WO(SO_4)_2$ indicates a more complicated decomposition scheme. First, a small amount of adhesive sulfuric acid (~2% of mass) is blown off, which is complete at 200 °C. The decomposition of $WO(SO_4)_2$ then starts at 270 °C, with a large endothermic peak at 326 °C. At around 350 °C, the decomposition slows down, clearly visible in the smaller gradient of the TG curve. At 425 °C, a small endothermic peak becomes

(26) Kato, K. *Acta Crystallogr., Sect. B* **1976**, *32*, 764–767.
(27) Holleman, A. F.; Wiberg, N. *Lehrbuch der Anorganischen Chemie, 102*; de Gruyter: Berlin, Germany, 2007.

apparent in the DTA curve, and finally the decomposition is complete at 530 °C with an exothermic step at 515 °C. The end product has been analyzed by means of X-ray powder diffraction and could be identified as the monoclinc modification of WO_3 reported by Loopstra and Boldrini.[28] The crystallinity of the decomposition product is high, as can be seen from the sharp reflections in the powder pattern. The intermediates of the decomposition between 350 and 530 °C could not be identified; most likely they are oxide-richer tungsten oxide sulfates. Quite uncommon is the exothermic decomposition step at 515 °C; the decay of a tungsten oxide sulfate into WO_3 and SO_3 should be expected to be an endothermic process.

$Re_2O_5(SO_4)_2$−I is the most temperature labile compound. The decomposition starts at 206 °C with a first endothermic maximum in the DTA curve at 242 °C. At a temperature of 306 °C, a second endothermic peak can be observed. At 335 °C, the decomposition is complete, leaving no residual products. The degradation mechanism of $Re_2O_5(SO_4)_2$ can only be speculated about. Most likely is the loss of two molecules of sulfur trioxide, leading to Re_2O_7 as an initial step. The Re_2O_7 itself melts at 300 °C, which explains the second DTA peak.[27] Finally, the Re_2O_7 volatilizes in the N_2 stream of the DTA/TG apparatus (bp of Re_2O_7: 360 °C).[27]

The thermal decomposition of $Re_2O_5(SO_4)_2$−II is also a two-step process, but in contrast to $Re_2O_5(SO_4)_2$−I, a reasonably stable intermediate is formed. The disintegration of $Re_2O_5(SO_4)_2$−II starts at 206 °C with the endothermic loss of one SO_3 molecule per formula unit, which is complete at 260 °C (peak maximum at 233 °C). With respect to the observed loss of mass, the intermediate can be assigned the composition $Re_2O_6(SO_4)$. At 270 °C, $Re_2O_6(SO_4)$ starts to lose the second SO_3 molecule, so finally Re_2O_7 is formed. Like in $Re_2O_5(SO_4)_2$−I, the Re_2O_7 vaporizes immediately in the stream of N_2. The observed strong peak in the DTA-curve at 341 °C is in good accord with the melting and boiling temperatures of Re_2O_7. Finally, the decomposition is complete at 365 °C and leaves virtually no residue (~1% of weight). Results of the thermogravimetric measurements and differential thermal analysis are presented in Figure 16.

3.3. Discussion. The crystal structures of $Nb_2O_2(SO_4)_3$, $MoO_2(SO_4)$, $WO(SO_4)_2$, and $Re_2O_5(SO_4)_2$−I and −II have some features in common, which should be discussed.

The first thing to mention is the tendency of the refractory metals to build [M=O] moieties. This behavior can easily be understood from the perspective of reducing the effective positive charge on the metal ion. For metals with an oxidation state larger than +IV, the formation of the pure sulfate compound $M(SO_4)_n$ is highly penalized over the oxide sulfates $MO_m(SO_4)_{(n-m)}$; the following equilibria can be assumed:

$$M(SO_4)_n \rightleftharpoons MO(SO_4)_{(n-1)} + SO_3 \rightleftharpoons MO_2(SO_4)_{(n-2)} + 2SO_3 \rightleftharpoons \ldots \rightleftharpoons MO_n + nSO_3 \quad (1)$$

Which species exists directly after dissolution of the metal chloride or oxide in sulfuric acid can only be speculated about. At low temperatures, monomeric sulfato complexes of the type $[M(SO_4)_n]^{m-}$ or $[MO(SO_4)_n]^{m-}$ are most likely, which have been isolated and characterized for niobium, tantalum, and molybdenum, e.g., $[M(SO_4)_6]^{7-}$ in $K_7[M(SO_4)_6]$ (M = Nb, Ta)[29] or $[MoO_2(SO_4)_4]^{4-}$ in $K_4[MoO_2(SO_4)_3]$.[30] At higher temperatures, the equilibria in eq 1 should be adjusted to oxide-richer compounds. Further heating leads gradually to the elimination of more SO_3 molecules, and finally the pure metal oxide is formed, which has been observed during the thermal decomposition of all compounds. Besides the temperature, the concentration of SO_3 in the sulfuric acid has an essential influence on the ratio between oxide and sulfate ions in the compounds formed. A higher SO_3 concentration moves the equilibria in eq 1 toward the left side and sulfate-richer compounds. In concentrated sulfuric acid, for example, niobium forms an oxide sulfate of the composition $Nb_2O_3(SO_4)_2 \cdot 0.25H_2O$,[4] whereas from sulfuric acid containing 25% SO_3, the sulfate-richer compound $Nb_2O_2(SO_4)_3$ can be isolated. From solutions of

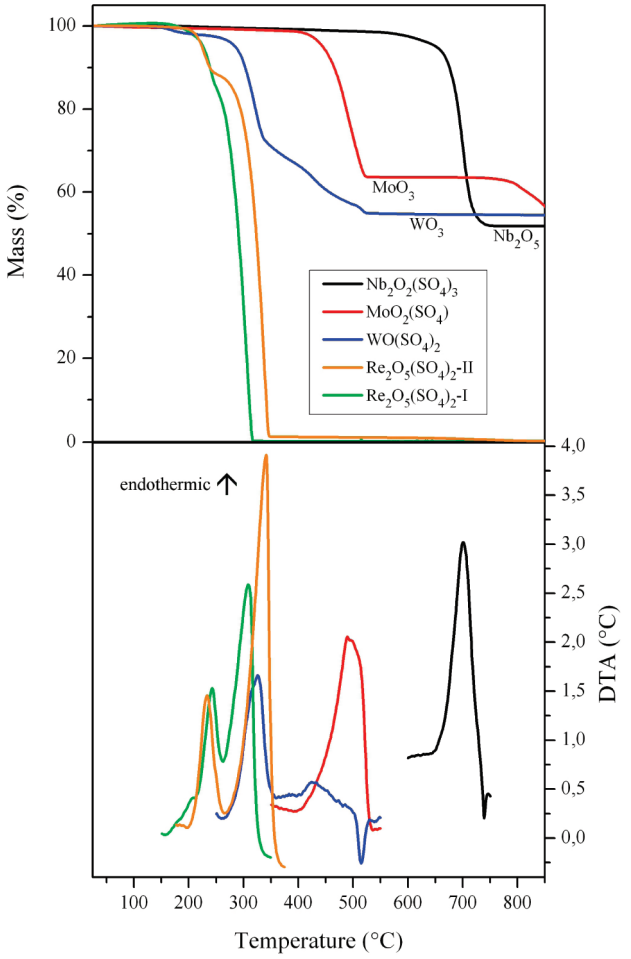

Figure 16. Results of the thermogravimetric measurements (top) and differential thermal analysis (below) for $Nb_2O_2(SO_4)_3$, $MoO_2(SO_4)$, $WO(SO_4)_2$, and $Re_2O_5(SO_4)_2$−I and −II. For clarity reasons, only the relevant parts of the DTA curves are plotted. The full graphs are available as Supporting Information.

(28) Loopstra, B. O.; Boldrini, P. *Acta Crystallogr., Sect. C* **1966**, *21*, 158–162.

(29) Borup, F.; Berg, R. W.; Nielsen, K. *Acta Chem. Scand.* **1990**, *44*, 328–331.

(30) Cline Schäffer, S. J.; Berg, R. W. *Acta Crystallogr., Sect. E* **2008**, *64*, i20.

SO_3 in sulfuryl chloride, the preparation of the again sulfate-richer compound $Nb_2O(SO_4)_4$ has been claimed.[6] Finally, the charge of the metal ion has an important influence on the ammount of oxide ligands in the compounds formed. Rhenium, for instance, has a higher tendency toward oxide-richer sulfates compared to the elements in groups 5 and 6. Even in sulfuric acid containing 65% SO_3 at moderate temperatures, no isolation of a more sulfate-rich compound than $Re_2O_5(SO_4)_2$ was possible.

In all cases, the metal ion is able to reduce its high positive charge of +V to +VII much better, if an oxide ligand is able to push the electron density toward the metal through additional π-donation. In the literature, the bond to the terminal oxide ligand in molecular compounds like oxide chlorides or coordination compounds is usually described as a M=O double bond, which has recently been confirmed by theoretical studies.[31] This is easily reflected in the short M=O distance. Interestingly, in the oxide sulfates, the M=O bond length is virtually independent from the nature and the charge of the metal ion. The M=O distance ranges between 167 and 169 pm regardless of whether the oxide ligand is bonded to Nb^{V}, Mo^{VI}, W^{VI}, or Re^{VII}.

The terminal oxide ligands play an important role in the crystal structure of $Nb_2O_2(SO_4)_3$, $MoO_2(SO_4)$, $WO(SO_4)_2$, and $Re_2O_5(SO_4)_2$−I and −II. They are involved in the strong distortion of the coordination polyhedra around the metal ions, which reflects short M=O distances for example. These distortion effects are typically found for octahedrally coordinated d^0 transition metal ions in contrast to main group metal ions of comparable size and charge. In solid state chemistry, these d^0 distortions play a crucial role, e.g., for nonlinear optical effects, and have been studied intensively. The main focus has been on understanding the influence of these distortions on the structures and properties of solid phases like binary and ternary oxides of d^0 metal ions. There are various parameters which influence the degree of distortion, like the bond network around the d^0 ion, structural incommensurations, cation−cation repulsion, and finally electronic effects.[32] According to Kunz and Brown, the separation of these effects is not trivial, as they influence each other, but only the bond network and cation−cation repulsions are able to direct the distortion. However, the electronic effect is the determining parameter of the degree of distortion, especially for d^0 ions with a small HOMO−LUMO gap like the small and highly charged V^{5+} and Mo^{6+} ions.

The electronic distortion component of octahedrally coordinated d^0 transition metal ions is usually explained on the basis of the second-order Jahn−Teller theorem.[33−35] The SOJT distortions can occur in systems with a nondegenerate ground state interacting with a low-lying excited state, e.g., if a small HOMO−LUMO gap in combination with a symmetry-allowed distortion is present. In octahedral d^0 complexes of high valent transition metals, the SOJT distortion manifests in a displacement of the metal atom from the ideal position in the octahedron center toward a vertex, an edge, or a face of the polyhedron. Through this distortion, a mixing of the empty metal d orbitals and the ligand p orbitals becomes possible, leading to a breakup of their degeneracy.

Since a distorted octahedral coordination environment is a common feature of the early transition metal d^0 ions Ti^{4+}, Zr^{4+}, Hf^{4+}, V^{5+}, Nb^{5+}, Ta^{5+}, Mo^{6+}, and W^{6+}, Halasyamani et al. and Alvarez et al. did a detailed analysis of the SOJT distortion effects in more than 750 compounds of these cations (oxides, compounds containing complex oxo-anions).[36] The authors quantified both the degree of the metal off-center displacement and the directional distortions (vertex, edge, face) in the $[MO_6]$ octahedra. They classified these cations into three groups, the strong distorters Mo^{6+} and V^{5+}; the intermediates W^{6+}, Ti^{4+}, Nb^{5+}, and Ta^{5+}; and Zr^{4+} and Hf^{4+}, which tend to nearly undistorted structures.

We did a similar examination of the $[MO_6]$ octahedra in the refractory metal oxide sulfates and compared the results with the literature averages for the respective metal cations from Halasyamani et al. and Alvarez et al. (Figure 17). For $MoO_2(SO_4)$, the off-center displacement of the metal ion in the respective polyhedra is in good accord with the literature averages found for Mo. Although the tungsten atom in $WO(SO_4)_2$ is in 7-fold coordination, the off-center displacement of W in the pentagonal bipyramid is comparable to the literature averages for octahedral d^0 tungsten complexes. In both Re oxide sulfates, the degree of the off-center displacement is of similar magnitude and lies between the strong distorters Mo^{6+} and V^{5+} and the intermediates W^{6+} to Ta^{5+}. This is in good accord with the results of Woodward et al., who showed that the degree of the distortions increases with increasing electronegativity of the metal ($EN_{Mo} = 2.16$, $EN_W = 1.7$, $EN_{Nb} = 1.6$, and $EN_{Re} = 1.9$).[37] This is quite interesting, as the energy of the empty d orbitals lowers with the metal cation becoming smaller and more highly charged. Hence, the HOMO−LUMO gap is expected to decrease, which should intensify the electronic effect on the distortion.[32] The off-center displacement of both Nb atoms in $Nb_2O_2(SO_4)_3$ is much larger ($r^2 = 0.090$ Å^2) than would be expected from the literature average value of 0.053 Å^2.

For the refractory metal oxide sulfates, the directional distortions of the cations are highly correlated with the amount of terminal oxide ligands in the respective coordination polyhedron. For compounds containing one oxide ligand per metal ion, which is the case for $Nb_2O_2(SO_4)_3$ and $WO(SO_4)_2$, distortions toward a vertex are found, whereas in $MoO_2(SO_4)$ and both modifications of $Re_2O_5(SO_4)_2$ with two oxide ligands coordinated to the metal ion, a distortion toward the edge formed by these ligands is the case. These findings are in good accord with the results of Halasyamani et al. and Alvarez et al., who reported a strong affection of Mo^{6+} for distortion toward an edge and a slight tendency of Nb^{5+} to distort in the direction of a vertex.[36] For W^{6+}, a preference for distortion

(31) Michalak, A.; DeKock, R. L.; Ziegler, T. *J. Phys. Chem. A* **2008**, *112*, 7256–7263.
(32) Kunz, M.; Brown, I. D. *J. Solid State Chem.* **1995**, *115*, 395–406.
(33) Öpik, U.; Pryce, M. H. L. *Proc. R. Soc. London, Ser. A* **1957**, *238*, 425–447.
(34) Pearson, R. G. *J. Am. Chem. Soc.* **1969**, *91*/*18*, 4947–4955.
(35) Pearson, R. G. *THEOCHEM* **1983**, *103*, 25–34.
(36) Ok, K. M.; Casanova, D.; Llunell, M.; Alemany, P.; Alvarez, S.; Halasyamani, P. S. *Chem. Mater.* **2006**, *18*, 3176–3183.
(37) Eng, H. W.; Barnes, P. W.; Auer, B. M.; Woodward, P. M. *J. Solid State Chem.* **2003**, *175*/*1*, 94–109.

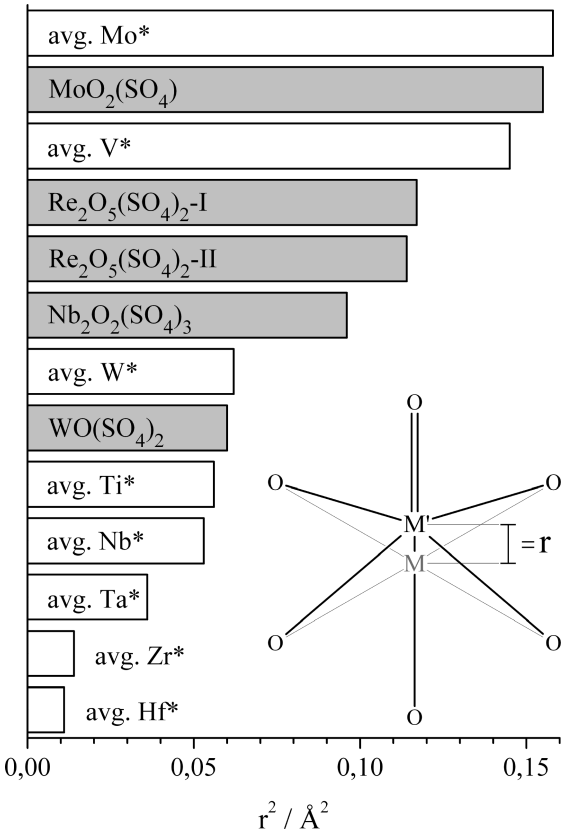

Figure 17. Plot of the octahedron distortion as a consequence of the second-order Jahn−Teller effect. The off-center displacement of the metal atom inside the octahedron is given as the square of the displacement vector's modulus r^2. The values marked with an asterisk are averaged values calculated by Halasyamani et al. and Alvarez et al. from at least 75 literature known compounds of the respective element.[36] The values calculated for the refractory metal oxide sulfates are in good accord with the literature averages for Mo and W, but the distortion of the [NbO_6] octahedra in $Nb_2O_2(SO_4)_3$ is much more pronounced. As the degree of the octahedron distortion is approximately correlated with the electronegativity of the metal, the results for both rhenium oxide sulfates conform with the EN of Re (1.9), lying between Nb (1.6) and Mo (2.16).

toward an edge has been reported, which does not apply to $WO(SO_4)_2$, probably due to the 7-fold coordination of the tungsten atom in this compound.

The M=O···M distance from the oxide ligand of one [M=O] moiety to the metal atom of a neighboring one is large and ranges from weak interactions in $Nb_2O_2(SO_4)_3$, $MoO_2(SO_4)$, and both modifications of $Re_2O_5(SO_4)_2$ (shortest M=O···M distance = 364−388 pm) to virtually no interactions in $WO(SO_4)_2$ (shortest M=O···M distance = 457 pm). This is a direct consequence of the strong metal−oxygen bond in the [M=O] moieties. Hence, the oxide ions are best described as a terminal ligand; i.e., no real M−O−M bridging takes place (except the bridging oxide ligand of the [Re_2O_5] moiety in $Re_2O_5(SO_4)_2$, of course). Instead, in the crystal structure of all compounds presented in this work, the [M=O] groups are facing each other, which leads to either the development of cavities in which the M=O groups are oriented like in $Nb_2O_2(SO_4)$ and $MoO_2(SO_4)$ or to the formation of layer structures found in $WO(SO_4)_2$ and both modifications of $Re_2O_5(SO_4)_2$. In these cases, the oxide ligands are located on the surface of these layers. Typical for these layer-type structures are the weak interactions between noncoordinating oxygen atoms of sulfate tetrahedra and the metal atoms from the neighboring layers, which are responsible for the cohesion between the layers. In typical solid state compounds of high valent metals like binary/ternary oxides, this behavior of the oxide ligands is not as distinct. Although short M−O distances indicating a strong covalent M=O bond are observed, these oxide ligands coordinate to adjacent metal atoms anyway. The formation of layered structures or structures containing significant cavities is observed seldomly; instead pronounced three-dimensional structures are formed.[38,39]

In the coordination chemistry of high valent refractory metal ions, the formation of [M=O] moieties with short M−O distances is most common. The bonding in these oxido complexes is well understood and usually formulated as a metal−oxygen multiple bond made up of a σ bond between oxygen and the metal ion paired with additional π donation from the oxide ligand toward the metal.[40,41] This multiple bond formalism is in good accord with the usually short M=O distance ranging between 160 and 180 pm. The [M=O] moieties in the refractory metal oxide sulfates have a close relationship to metal−oxido complexes of these elements. For example, they share the short metal−oxygen bond, whose length of around 168 pm for the refractory metal oxide sulfates is in good accord with values found in coordination compounds. Another analogy is the behavior of the oxide ligand, which is monodentate and does not interact with a second metal atom. In coordination compounds of high valent transition metals, octahedral distortions are also present; commonly they reflect a lengthening of the bond to the ligand in the *trans* position toward the oxide ligand. Due to the competition for the same metal orbital, the strong M=O bond leads to a significantly weakened (and therefore lenghtened) bond to the ligand in the *trans* position of the oxide ligand (also known as *trans* lengthening or the structural *trans* effect).[42,43] In order to categorize the magnitude of the *trans* lengthening for the refractory metal oxide sulfates, the degree of bond lengthening to the ligand in the *trans* position has been plotted in dependency on the metal's valence in Figure 18.

The degree of *trans* lengthening seems to depend on the charge of the metal ion in the respective compound. For $Nb_2O_2(SO_4)_3$, the elongation of the bond to the ligand in the *trans* position toward the [Nb=O] moiety (average 235 pm) is about 11 pm larger than in the oxide sulfates of group 6 (224 pm) and 17 pm larger than in both modifications of $Re_2O_5(SO_4)_2$ (218 pm). Probably, this effect can be assumed to be a consequence of the increasing positive charge of the metal ion in the order Nb^{V}, Mo^{VI}/W^{VI}, Re^{VII}, which leads to a contraction of the metal d orbitals and therefore to shorter M−O bonds. These results are somewhat astonishing, as the magnitude of the *trans* lengthening (Nb > Mo, W > Re) is in conflict with the prediction of the degree of distortion of the [MO_6] octahedra

(38) Müller-Buschbaum, H. *Z. Anorg. Allg. Chem.* **2007**, *633*, 2491–2522.
(39) Müller-Buschbaum, H. *Z. Anorg. Allg. Chem.* **2008**, *634*, 2111–2124.
(40) Ballhausen, C. J.; Gray, H. B. *Inorg. Chem.* **1962**, *1*/*1*, 111–122.
(41) Gray, H. B.; Hare, C. R. *Inorg. Chem.* **1962**, *1*/*2*, 363–368.
(42) Shustorovich, E. M.; Porai-Koshits, M. A.; Buslaev, Y. A. *Coord. Chem. Rev.* **1975**, *17*, 1–98.
(43) Coe, B. J.; Glenwright, S. J. *Coord. Chem. Rev.* **2000**, *203*, 5–80.

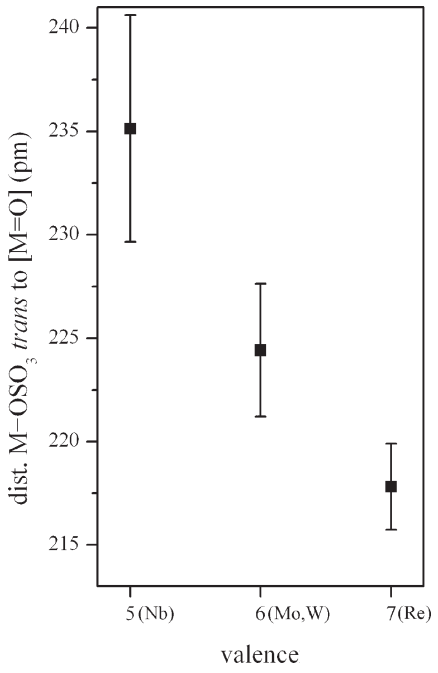

Figure 18. Left: Elongation of the M−OSO_3 bond *trans* to the oxide ligand in the refractory metal oxide sulfates plotted in dependency on the oxidation state of the metal ion. Note: These values are averaged over all crystallographically different metal atoms in the crystal structures of the respective compounds.

from the second-order Jahn−Teller distortion calculation averages (Mo > Re > W > Nb).[36]

However, the model of the structural *trans* effect seems to be another description possibility of the electronic effect on the distortion, like the second-order Jahn−Teller theorem. Both models assume an electron donation from ligand p orbitals into the empty transition metal d orbitals, and both models deliver an explanation of the electronic distortion effects around d^0 transition metal ions. But as the refractory metal oxide sulfates are polymeric solid state compounds, and not comprised of discrete molecules, other effects like lattice stresses and cation−cation repulsion cannot be neglected. In combination with the electronic second-order Jahn−Teller distortion, these combined effects are the primarily source of the irregular coordination spheres found around the metal ions in the refractory metal oxide sulfates.

Although the number of structurally characterized pseudobinary oxide sulfates of the refractory metals is rather limited, a comparatively large number of compounds with other complex oxo-anions is described in the literature. In large part, these are oxide phosphates, whose structural similarities and differences from the respective oxide sulfates should be discussed. Simple orthophosphates of the type $M_xO_y(PO_4)_z$ are known for Nb, Ta, Mo, W, and Re. A widespread structure type is $MO(PO_4)$, which exists in a tetragonal as well as an orthorhombic modification and is found for the quinquevalent cations of Nb, Ta, Mo, and W. Both $TaO(PO_4)$ and $MoO(PO_4)$ crystallize in the tetragonal setting,[44,45] $WO(PO_4)$ in the orthorhombic crystal system,[46] and $NbO(PO_4)$ exists in both modifications.[47,48] In both polymorphs, oxide ions connect the refractory metal atoms to chains, although in tetragonal $MO(PO_4)$, the M−O−M bridges are linear but asymmetric (one long M−O distance of 230−260 pm, one short M−O distance of 165−180 pm), and in orthorhombic $MO(PO_4)$, zigzag chains with symmetric M−O−M bridges are formed (M−O distance around 185 pm). A three-dimensional structure is formed by connection of these chains through phosphate anions. The major difference between these compounds and the refractory metal oxide sulfates is the occurrence of polymeric ···M−O−M··· chains, which is eminently the case for the orthorhombic modification of $MO(PO_4)$, although the tendency toward [M═O] groups foreshadows the crystal structure of monoclinic $MO(PO_4)$.

Other examples of simple oxide phosphates are $W_2O_3(PO_4)_2$, which exists in a monoclinic as well as an orthorhombic form,[49,50] and the orthorhombic $Re_2O_3(PO_4)_2$.[51] Both modifications of $W_2O_3(PO_4)_2$ contain discrete $[W_2O_3]$ units, which are interconnected through phosphate tetrahedra to a three-dimensional network. Each tungsten atom is coordinated by four phosphate ions, one bridging oxygen atom, and one terminal oxide ligand. The terminal oxide ligands do not interact with neighboring tungsten atoms, so the W═O distance is expectedly short (161−174 pm). The lattice parameters of $Re_2O_3(PO_4)_2$ are related to the ones found for orthorhombic $W_2O_3(PO_4)_2$, but the structure exhibits some differences. The crystal structure contains similar $[Re_2O_3]$ units, but the coordination of the Re atoms differs. Besides one terminal and one bridging oxide ligand, each rhenium atom is coordinated by four phosphate ions, but in contrast to $W_2O_3(PO_4)_2$, one phosphate tetrahedron acts as a chelating ligand toward the $[Re_2O_3]$ moiety.

Both $W_2O_3(PO_4)_2$ and $Re_2O_3(PO_4)_2$ have a considerable relationship toward both modifications of $Re_2O_5(SO_4)_2$. On the one hand, the oxide sulfates and phosphates have the same metal to oxo-anion ratio; on the other hand, both contain the unique $[M_2O_{11}]$ octahedra dimer. Of course, the major difference is the higher charge of the metal and the less negative charge of the oxo-anion in the Re^{VII} oxide sulfates. This leads to a difference in the amount of terminal oxide ligands per metal ion. However, the bidentate coordination mode of phosphate toward the $[Re_2O_3]$ moiety found in $Re_2O_3(PO_4)_2$ is also realized for both oxide sulfates ($Re_2O_5(SO_4)_2$−I, two chelating $[SO_4]$ tetrahedra; $Re_2O_5(SO_4)_2$−II, one chelating $[SO_4]$ tetrahedra). Furthermore, the geometry of the Re−O−Re bridge in $Re_2O_3(PO_4)_2$ (Re−O−Re angle, 161°; Re−O dist, 184 pm) is similar to the values found for both modifications of $Re_2O_5(SO_4)_2$ (I, 149° and 188 pm; II, 161° and 187 pm).

In summary, refractory metal oxide sulfates and phosphates share the tendency toward polymeric structures, which is most likely a consequence of the numerous

(44) Longo, J. M.; Pierce, J. W.; Kafalas, J. A. *Mater. Res. Bull.* **1971**, *6*, 1157–1166.
(45) Kierkegaard, P.; Westerlund, M. *Acta Chem. Scand.* **1964**, *18*, 2217–2225.
(46) Wang, S. L.; Wang, C. C.; Lii, K. H. *J. Solid State Chem.* **1989**, *82*, 298–302.
(47) Longo, J. M.; Kierkegaard, P. *Acta Chem. Scand.* **1966**, *20*, 72–78.
(48) Serra, D. L.; Hwu, S. Y. *Acta Crystallogr., Sect. C* **1992**, *48*, 733–735.
(49) Kierkegaard, P.; Åsbrink, S. *Acta Chem. Scand.* **1964**, *18*, 2329–2338.
(50) Hanawa, M.; Imoto, H. *J. Solid State Chem.* **1999**, *144*, 325–329.
(51) Islam, S. M.; Glaum, R. *Z. Anorg. Allg. Chem.* **2009**, *635*, 1008–1013.

linking possibilities provided by the four oxygen atoms in the $[EO_4]^{n-}$ anion. Nevertheless, the refractory metal oxide sulfates have a higher tendency toward the formation of layer-type structures. This is obviously a consequence of the [M=O] moieties, as the oxide ligands in the refractory metal oxide sulfates have a lesser tendency toward the formation of M−O−M bridges.

The thermal stability of a refractory metal oxide sulfate seems to depend primarily on the charge of the corresponding metal ion. The decomposition temperature decreases drastically from 650 to 206 °C in the order Nb^{V}, Mo^{VI}/W^{VI}, Re^{VII}. Another important parameter is the amount of oxo-anions per formula unit. In most cases, the decomposition temperature decreases with an increasing abundance of oxo-anions in the compound. For example, the degradation of $WO(SO_4)_2$ (T_S = 270 °C) starts around 130 °C earlier than the decomposition of the oxide-richer $MoO_2(SO_4)$. The thermal decomposition characteristics of the refractory metal oxide sulfates can easily be understood with the equilibrium (eq 1) in mind: A compound with a higher content of oxo-anions (and therefore fewer π-donating oxide ligands) has a higher tendency of losing SO_3 to gain additional oxide ligands. Likewise, a high valent metal has a stronger demand to compensate its high positive charge, so the liberation of SO_3 under the formation of oxide-richer compounds at comparatively moderate temperatures is the logical consequence. Finally, the last step in this process is the formation of the pure metal oxide.

Interestingly, during the thermal decomposition measurements, another effect of the refractory metal's nature on the properties of its corresponding oxide becomes apparent: The oxides of niobium and tungsten formed by the decomposition of $Nb_2O_2(SO_4)_3$ and $WO(SO_4)_2$ are stable beyond 1050 °C, whereas MoO_3, as product of the decomposition of $MoO_2(SO_4)$, melts at 790 °C and volatizes nearly completely up to 1050 °C. For rhenium, the results are much more extreme; Re_2O_7, the product of the decomposition of both Re oxide sulfates, volatized completely below 400 °C. Again, the increasing charge of the metal ion plays the essential role; here, it leads to an increase of the covalency of the M−O bond in the particular oxides. Finally, the row Nb_2O_5, WO_3, MoO_3, and Re_2O_7 are good examples for the transition of the rather ionic oxides (Nb, W) to a pure molecular compound (Re). Molybdenum is a borderline case.

3.4. Conclusion. An aim of this work was to study properties of refractory metal sulfates as possible precursors for the generation of the corresponding metal oxides. For this purpose, the oxide sulfates $Nb_2O_2(SO_4)_3$, $MoO_2(SO_4)$, $WO(SO_4)_2$, and $Re_2O_5(SO_4)_2$−I and −II have been synthesized and characterized with the main focus on the crystal structure and thermal decomposition. From the structure analysis, the tendency of the refractory metals to form oxide sulfates, which contain [M=O] moieties with short M−O distances and a covalent character, became apparent. The oxide ligands have a structure dominating effect, which reflects the formation of layer-type structures or networks containing noticeable cavities. From this point of view, a derivatization of the oxide ions with comparable ligands, e.g., nitride or fluoride, should be considered.

The eligibility of refractory metal oxide sulfates as precursors for the deposition of the metal oxides is somewhat restricted. In fact, they deliver the respective metal oxide as a decomposition residue, but either their decomposition temperature is too high (Nb, Mo, W) or the metal oxide volatizes during the decomposition process (Re).

Acknowledgment. The authors thank Mr. Wolfgang Saak for the collection of the X-ray data. We also thank the "Fonds der chemischen Industrie" and the "Heinz-Neumüller-Stiftung" for granting a stipend to U.B. Funding through the "Deutsche Forschungsgemeinschaft" is gratefully acknowledged.

Supporting Information Available: Tables S1−S20 contain the complete crystallographic data (measurement and refinement procedure, atom coordinates, bond lengths and angles, anisotropic displacement parameters) for all compounds. Figures S1−S5 contain the complete plots for the thermogravimetric and differential thermal analysis data; Figures S6 and S7 show the powder pattern of the decomposition products of $Nb_2O_2(SO_4)_3$ and $WO(SO_4)_2$. Crystallographic information files are also provided. This material is available free of charge via the Internet at http://pubs.acs.org.